ADAPTIVE OPTICS CORRECTIONS IN IMPROVING THE BEAM SPREAD IN UNDERWATER TURBULENT MEDIUM

MELİSA NUR TÜRKYILMAZ

AUGUST 2022

ÇANKAYA UNIVERSITY

GRADUATE SCHOOL OF NATURAL AND APPLIED SCIENCES

DEPARTMENT OF ELECTRICAL AND ELECTRONICS ENGINEERING

MASTER'S THESIS IN

ELECTRICAL AND ELECTRONICS ENGINEERING

ADAPTIVE OPTICS CORRECTIONS IN IMPROVING THE BEAM SPREAD IN UNDERWATER TURBULENT MEDIUM

MELİSA NUR TÜRKYILMAZ

AUGUST 2022

ABSTRACT

ADAPTIVE OPTICS CORRECTIONS IN IMPROVING THE BEAM SPREAD IN UNDERWATER TURBULENT MEDIUM

TÜRKYILMAZ, Melisa Nur
M.Sc., Department of Electrical-Electronics Engineering
Supervisor: Prof. Dr. Yahya Kemal BAYKAL

August 2022, 77 pages

The popularity of the underwater wireless optical communication has increased recently because optical systems have the advantage of providing transmission at high data rates with low latency. However, UWOC is challenging due to harsh environmental conditions and one of the main effects of in oceanic medium is the turbulence. Turbulence causes increase in the beam spread which reduces the performance of the UWOC. In this thesis, the effectiveness of adaptive optics correction for Gaussian beams in oceanic turbulence is studied. The beam size and beam spread were examined with adaptive optics method. The reductions in beam size and beam spread indicate that the adaptive optics correction is a very effective method for reducing the turbulence-caused signal degradations. When investigating the effect of underwater turbulence, the power spectrum in the oceanic medium is supposed to be isotropic and homogeneous. Using the extended Huygens Fresnel principle, average intensity is found. The beam size and beam spread were observed utilizing Carter's definition. Piston, focus, tilt and astigmatism components of adaptive optics corrections were utilized to find the beam size and the beam spread in turbulent oceanic medium. The reduction in the beam size and beam spread was investigated against the ratio of temperature to salinity contributions to the refractive index spectrum, rate of dissipation of mean squared temperature, rate of

dissipation of kinetic energy per unit mass of fluid, inner scale, receiver aperture diameter, link length, source size and the wavelength. This reduction was compared with and without the adaptive optics method. Using the MATLAB program, graphs were presented and calculations were performed. In this thesis, it is aimed to provide the most suitable conditions for beam propagation in underwater turbulent environment and to increase the UWOC performance.

Keywords: Underwater Wireless Optical Communication, Turbulent Oceanic Medium, Beam Spread, Beam Size, Adaptive Optics.

ÖZ

TÜRBÜLANSLI SUALTI ORTAMINDA IŞIN YAYILIMINDA UYARLANABİLİR OPTİK DÜZELTMELER

TÜRKYILMAZ, Melisa Nur
Yüksek Lisans, Elektrik-Elektronik Mühendisliği Anabilim Dalı
Tez Yöneticisi: Prof. Dr. Yahya Kemal BAYKAL

Ağustos 2022, 77 sayfa

Optik sistemlerin düşük gecikme ile yüksek veri hızlarında iletim sağlama avantajına sahip olması nedeniyle, su altı kablosuz optik iletişiminin popülaritesi son zamanlarda artmıştır. Bununla birlikte, UWOC sert çevre koşulları nedeniyle zorludur ve okyanus ortamındaki ana etkilerden biri türbülanstır. Türbülans, ışın yayılımında artışa neden olur ve UWOC'nin performansını düşürür. Bu tezde, okyanus türbülansında Gauss ışınları için uyarlanabilir optik düzeltmenin etkinliği incelenmiştir. Uyarlanabilir optik yöntemi ile ışın boyutu ve ışın yayılımı incelenmiştir. Işın boyutundaki ve ışın yayılımındaki azalmalar, uyarlanabilir optik düzeltmenin türbülansın neden olduğu sinyal bozulmalarını azaltmak için çok etkili bir yöntem olduğunu göstermektedir. Sualtı türbülansının etkisi araştırılırken, okyanustaki güç spektrumunun homojen ve izotropik olduğu varsayılır. Işık şiddeti yoğunluğu, genişletilmiş Huygens-Fresnel ilkesi uygulanarak elde edildi. Işın boyutu ve ışın yayılımı, Carter'ın tanımı kullanılarak gözlemlendi. Uyarlanabilir optik düzeltmelerinin piston, eğim, odak ve astigmatizma bileşenleri, türbülanslı okyanus ortamında ışın boyutuna ve ışın yayılımına uygulandı. Işın boyutundaki ve ışın yayılmasındaki azalma, sıcaklığın tuzluluğa oranının kırılma indisi spektrumuna katkılarına, ortalama kare sıcaklığın dağılma hızına, sıvının birim kütlesi başına kinetik enerjinin dağılma hızına, iç ölçeğe, alıcı açıklık çapına, bağlantı uzunluğuna, kaynak boyutuna ve dalga boyuna karşı değerlendirildi. Bu azalma adaptive optik

metodu kullanılarak ve kullanılmayarak mukayese edildi. MATLAB programı kullanılarak grafikler sunulmuş ve hesaplamalar yapılmıştır. Bu tezde, sualtı türbülanslı ortamda ışın yayılımı için en uygun koşulların sağlanması ve UWOC performansının artırılması amaçlanmıştır.

Anahtar Kelimeler: Sualtı Kablosuz Optik Haberleşme, Türbülanslı Okyanus Ortamı, Işın Yayılımı, Işın Boyutu, Uyarlanabilir Optik

ACKNOWLEDGEMENTS

I would like to express my sincere gratitude to Prof. Dr. Yahya Kemal BAYKAL for his supervision, special guidance, suggestions, and encouragement through the development of this thesis.

Finally, I would like to thank my parents with all my heart for their understanding, endless support and love.

TABLE OF CONTENTS

LIST OF FIGURES

LIST OF ABBREVIATIONS

ABBREVIATIONS

AO	:Adaptive Optics
AOF	:Adaptive Optics Filter
AUV	:Autonomous Underwater Vehicle
BER	:Bit Error Rate
FTVH	:Flat-Topped Vortex Hollow
Mbps	:Megabits per Second
MCF	:Mutual Coherence Function
ROV	:Remotely Operated Vehicle
TEM	:Transverse Electro-Magnetic
UWOC	:Underwater Wireless Optical Communication

CHAPTER 1

INTRODUCTION

1.1. BACKGROUND

The underwater wireless optical communication (UWOC) systems have become popular in the last few years because UWOC systems provide much higher data bit rate and low latency in underwater media over the classical acoustical communication systems [1]. UWOC systems are used in applications which need high data transmission and high bandwidth, such as military, security harbor inspections, underwater monitoring and surveillance sensor networks, autonomous underwater vehicles (AUVs), remotely operated vehicles (ROVs) and sensor networks [2-14]. The reason why the underwater wireless optical communication (UWOC) system is more advantageous than the classical acoustic system because acoustic and optical waves have different effects on underwater communication performance.

Due to the optical wireless communication's higher bandwith, it can provide higher data rates (up to hundreds of Mbps) [6,15-18] at low latency, whereas acoustic waves propagate slowly and this causes low data bit rates [19,20] at high latencies. Sound propagates in underwater at speed of approximately 1500 m/s so this causes high latency at long-range [5] and propagation occurs over multiple paths. The performance of acoustic communication is decreased by low bandwidth, high transmission loss, noise, multi-path propagation, doppler spread, and high latency [21-27]. Therefore, these limitations cannot support the use of bandwidth-hungry underwater applications such as image and real-time video transmission. However, since acoustic communication supports long-distance (up to kilometers) transmission [11,28], there are several studies to improve the performance of acoustic communication. [25,26,28,29]. Nevertheless, acoustic systems are susceptible to malicious attacks due to their bad performance such as high delay, low bandwidth

and high bit error rate [30]. With underwater acoustic communication, it is possible to reach tens of kbps data rate over long distances in kilometers and hundreds of kbps data rate over short distances in meters [6]. However, some underwater vehicles, observatories and sensor networks may require data rates of tens of Mbps or even higher. The utilization of copper cables and fiber optics may provide to obtain high data rates around Mbps but they require significant engineering [6]. On the other hand, they have maintenance and installation issues. For these reasons, the best alternative to achieve the high data rate, low latency, higher bandwidth and overcome the difficulties of acoustic communication systems is UWOC. [5,7,31-33]. In addition, UWOC provides secure links and is economical due to low installation costs. Besides all these advantages, the optical band is not involved in the telecommunications regulations so it does not require payment of licensing [34-40]. However, UWOC is more efficient for short distances because characteristics of the underwater medium cause the degradation of the optical wave so UWOC systems can only be effective at short distances of one hundred meters.

Propagation of the optical signal in underwater is affected by mainly three phenomena which are the absorbtion, scattering and oceanic turbulence [33,41-45]. Absorption and scattering result from the presence of sea water constituents, such as dissolved salts, chlorophyll, suspended particles and water molecules [46-48]. These two impairing effects cause power loss and deviation of light photons and highly attenuate the received optical signal. As a result, optical signals cannot propagate very far in underwater medium due to their decreased energy. In literature, the attenuation coefficient is expressed as the sum of the effects the absorbtion coefficient and scattering coefficient [49-51]. The water type is effective in changing these parameters. According to dissolved substances and geographical location (distance from ocean to shore), water has four different types. Namely, clear ocean water, pure seawater, turbid harbor water, and coastal ocean water [52-56]. The most suitable wavelength interval for UWOC systems to operate is from 450 nm to 550 nm which corresponds to the blue and green region of the visible light spectrum because, this interval provides the relatively minimum attenuation.

Turbulence is another challenge that significantly degrades the performance of the UWOC systems [57]. Changes in salinity, temperature, and density in ocean water lead to fluctuations in the refractive index and this creates turbulence in

underwater [58,59]. Nikishov and Nikishov introduced the power spectrum of refractive index fluctuations in oceanic medium and they determined the contribution of salinity and temperature fluctuations to the refractive index [60].

Many studies examined the effect of turbulence on various entities such as normalized intensity, average intensity, average transmittance and the scintillation index. By the Rytov method and the extended Huygens-Fresnel method average intensity was obtained [61-67]. There are several studies investigating normalized intensity and average intensity in the oceanic environment. For example, Flat-Topped Vortex Hollow (FTVH) [68], evolution behaviour of Gaussian-Schell model vortex beam [69], radial phase-locked partially coherent standard Hermite-Gaussian beam [70], Lorentz beam [71,72,73], Lorentz Gaussian [74], rotating elliptical Gaussian [75], partially coherent anomalous hollow vortex beam [76,77], radial phase-locked multi-Gaussian Shell-model [78], partially coherent model beams [58], phase-locked partially coherent radial flat-topped array laser [79], four-petal Gaussian model [80], radially polarized twisted Gaussian-Schell model [81], random electromagnetic multi-Gaussian Schell-model vortex beam [82], $M \times N$ Gaussian array [83], hollow Gaussian beam [84], multi-Gaussian Schell-model hollow vortex beams [85] and partially coherent flat-topped [67] beams are reported. Additionally, the average intensity and beam quality were analyzed in oceanic turbulence [86,87]. The intensity has also been investigated in several mediums other than the ocean. In turbulent atmospheric medium, the average intensity of cosine Gaussian [88], cosine-hyperbolic Gaussian [89] and flattened Gaussian beams [90] have beeen studied. Also, the intensity has also been involved in studies for turbulent biological tissues [91,92].

The average transmittance is another factor that shows the effect of turbulence [93,94]. In oceanic medium, by applying the transmitting probability of signal vortex modes, the effect of oceanic turbulence on the transmittance of the vortex modes carried by Mathieu-Gaussian beam [95], average transmittance for partially coherent flat-topped beam [67], transmittance of a finite-energy frozen beam [96], cos Gaussian and cosh-Gaussian beams [97] have been studied. Also, the effect of anisotropy on the transmittance for multi-Gaussian beam [98], the average transmittance in focused collimated laser beams [99] have been investigated.

Another difficulty in underwater turbulence which severely degrades the received optical signal is the intensity fluctuation (scintillation). In clear ocean, scintillations effects are generally more than absorption and scattering [100]. Scintillations have been evaluated for several beam types in oceanic medium. Some of these are the optical spherical and plane waves [101], Gaussian beams [102,103], partially coherent Gaussian [103], flat-topped beam [67], partially coherent flat-topped laser beam [104], higher-order mode laser beam [105-108], multimode laser beams [105], cross-beam [109], phase-locked partially coherent flat-topped array laser beam [110]. Also, scintillations are examined for multiple-input single-output optical links [111] and LED sources [112].

The other important phenomena studied in the underwater are the beam wander [113-115] and beam spreading [113,114,116-119]. The optical beam emanating from a transmitter propagates in vacuum and beam spreads when it reaches the receiver. If the turbulence of the medium increases, the beam size expands more. The beam spread is obtained when the beam size at the receiver in free space is subtracted from the beam size at the receiver in turbulence [92]. Beam spread can be investigated in a variety of turbulent environments such as the ocean, atmosphere and biological tissue. In underwater turbulence, beam spread calculated for various beam types such as Gaussian array beams [118], partially coherent flat-topped beams [67] and propagation properties of partially coherent anomalous hollow beams [76], Lorentz-Gauss vortex beam [119]. In atmospheric turbulence, beam spread is investigated for partially coherent beams [120], Lorentz-Gauss [121,122], elliptical Gaussian [123], partially coherent flattened Gaussian beams propagating through turbulence[124] and radial Gaussian array beams [125,126]. Morever, beam spread has recently been studied in biological tissues [91,92].

Several methods are utilized to reduce the damaging effects of turbulence on the beam propagation and to improve the performance of wireless optical communication. [104-106,127,128]. Some of these are the aperture averaging [129,130], spatial diversity [111,131,132], use of partially coherent source [104,133], beam shaping [105,109] and optical modulation [134-136]. The adaptive optics correction is one of the most successful techniques to enhance the propagation of beam and the performance of wireless optical communication. Adaptive optics method was first introduced in astronomy and medicine, then are used also in free-

space communication, remote sensing, directed energy and target recognition. By using the adaptive optics method, turbulence-caused signal distortions such as the scintillation and beam spread are reduced and the performance determining the metric Bit Error Rate (BER) is increased, thus improving the performance of the communication system. Adaptive optics method is addressed as a method to reduce the signal degradation by many researchers and is employed in several turbulent media. In this method, using deformable mirror to impose the opposite of the phase disturbance induced by turbulence, the effects of turbulence can be reversed [137]. In literature, applications of adaptive optics have been investigated in atmospheric turbulence [135,138-148], in oceanic turbulence [149–154] and in turbulent biological tissues [92]. The scintillation and BER performances were scrutinized with adaptive optics [151-154].

In this study, it is aimed to increase underwater communication system performance by examining the beam spread of Gaussian beam using adaptive optics method. Filter functions of adaptive optics are introduced and the reduction of the beam spread is evaluated. The beam spread are observed versus the ratio of temperature to salinity contributions to the refractive index spectrum ω, rate of dissipation of mean squared temperature χ_T, rate of dissipation of kinetic energy per unit mass of fluid ε, source size, receiving aperture diameter, link length and the wavelength. The components of the adaptive optics method is applied to the beam spread in the form of piston only (P only), tilt only (T only), focus only (F only), astigmatism only (A only), and tilt+focus+astigmatism+piston (T+F+A+P). The beam spread is examined by comparison with the corrected beam spread with and without adaptive optical filter (no AOF) by focusing on the reduction in beam spreads. If scintillation was observed, the effectiveness of adaptive optics refers to the capability of adaptive optics to decrease the scintillation. If the BER was evaluated, high BER performance shows us that adaptive optics (AO) is effective. In this study, the performance success of the system has been interpreted by considering how much reduction in beam spread through the adaptive optical filtering is achieved. The wavelength has been chosen as 532 nm because blue–green region is the least absorbed and scattered wavelength in underwater medium. MATLAB program was used to demonstrate numerical results.

1.2. OBJECTIVES

The motivation for this research is to clarify how effective the adaptive optics correction can be in improving underwater communication system performance and how it will affect optical beam propagation.

1.3. THESIS OUTLINE

In Chapter 2, the propagation of optical beam is explained. Turbulence formulation and effects of turbulence parameters are given. In Chapter 3, the beam size and beam spread in the oceanic turbulent medium analyzed and their formulas are given. In Chapter 4, the methodology of adaptive optics correction was explained and its effect on beam spread was demonstrated with its formulas. Chapter 5 focuses on showing the improvement in beam size and beam spread as a result of applying adaptive optics filters with the included graphics. In addition, the graphs in Chapter 5 show the influence of underwater turbulence parameters on the beam size and beam spread. Finally, this study was completed in the conclusion part of Chapter 6, with the evaluations made according to the results obtained.

CHAPTER 2

LASER BEAM PROPAGATION THROUGH OCEAN

2.1. OCEANIC TURBULENCE

Optical propagation in a turbulent ocean is challenging due to chaotic oceanic conditions. Turbulence is caused by the mobility and temperature of the liquid and the inorganic particles and dissolved organic proportions. Underwater turbulence causes the signal degradation and reduces wireless optical communication performance. Salinity, temperature, and mobility are important factors leading to turbulence. The salinity and temperature fluctuations cause to change the refractive index of water and the random variation of the index of refraction defines the optical turbulence. Also, variations of temperature and salinity determine the influence of underwater turbulence. They cause the signal degradation during the signal propagation in oceanic medium. Due to the complexity and chaotic conditions of the oceanic environment, optical beam propagation is more difficult in ocean turbulence than in atmospheric turbulence. Turbulence can be defined with three basic assumptions: stationary, homogeneous and isotropic. In this thesis the power spectrum of oceanic turbulence is homogeneous and isotropic. It contains diffusion of salt and thermal diffusivity. According to this assumption, the power spectrum is expressed as [60].

$$\Phi_n(\kappa) = 0.388\times10^{-8}\varepsilon^{-1/3}\omega^{-2}\chi_{\mathrm{T}}\kappa^{-11/3}\left[1+2.35(\kappa\eta)^{2/3}\right]\psi(\kappa,\omega) \tag{2.1}$$

$$\Phi_n(\kappa) = 0.388C_m^2\omega^{-2}\kappa^{-11/3}\left[1+2.35(\kappa\eta)^{2/3}\right](\omega^2 e^{-A_T\delta}+e^{-A_S\delta}-2\omega e^{-A_{TS}\delta}) \tag{2.2}$$

where κ is the spatial frequency, ε is the rate of dissipation of kinetic energy per unit mass of fluid, η is the Kolmogorov micro scale length in m. Energy transfers are an important cause of turbulence. ε determines the turbulent dissipation which takes values in the range from 10^{-1} $\mathrm{m^2/s^3}$ to 10^{-10} $\mathrm{m^2/s^3}$. When ε is small, ocean turbulence is strong, when ε is large, ocean turbulence is weak. χ_{T} is the rate

of dissipation of the mean-squared temperature in K^2/s. Temperature provides information about the existence and movement of turbulent motion, relation to heat energy, density and its spatial variation. Values of χ_T vary in the ocean in the range from 10^{-4} K^2/s to 10^{-10} K^2/s. Larger χ_T value causes stronger turbulence and smaller χ_T value reflects weak turbulence. ω is the ratio of temperature and salinity contributions to the refractive index spectrum. It is a unitless parameter and takes values in the from -5 to 0 in underwater. If ω approaches -5, temperature-induced optical turbulence is dominant, and if ω approaches 0, salinity-induced optical turbulence is dominant. Temperature-induced optical turbulence is less effective than the salinity-induced optical turbulence. $A_T = 1.863\times10^{-2}$, $A_S = 1.9\times10^{-4}$, $A_{TS} = 9.41\times10^{-3}$ are constants and $\delta = 8.284(\kappa\eta)^{4/3} + 12.978(\kappa\eta)^2$.

2.2. GAUSSIAN BEAM WAVE

Gaussian beam can be defined as the solution of the paraxial Helmholtz equation. The lowest-order transverse electro-magnetic (TEM) Gaussian-beam wave is also called a TEM_{00} wave. The output from the ideal coherent laser source is assumed to be a Gaussian field profile and it corresponds to transverse electromagnetic field (TEM_{00} mode). Gaussian beam wave function at the transverse plane z = 0, also called the source plane, is given by

$$u(\mathbf{s}, z=0) = A\exp\left(-k\alpha|\mathbf{s}|^2\right), \tag{2.3}$$

where

$$\alpha = \frac{1}{2k\alpha_s^2} + \frac{i}{2F}, \tag{2.4}$$

λ is the wavelength in m , $k = 2\pi/\lambda$ is the wavenumber in m^{-1}, α_s is the source size in m, α is the complex parameter and it is related to the phase front radius of curvature and source size, $\mathbf{r}$ is the transverse coordinate at the receiver, $\mathbf{s} = (s_x, s_y)$ is transverse source coordinates A is the field amplitude in $(W/m^2)^{1/2}$ and F is the radius of curvature in m and also called as the focal length or phase front of curvature.

2.3. EXTENDED HUYGENS FRESNEL PRINCIPLE

In turbulent medium, laser beam field spreads and the extended Huygens-Fresnel principle is used to obtain the theoretical results of beam spread and beam size. The extended Huygens Fresnel principle is defined in Eq. (2.5) and it is a solution of the paraxial wave equation (in other words the parabolic equation). The extended Huygens Fresnel principle leads to obtain the optical field (also called as the beam footprint) in the receiver plane at a distance L from the source in a turbulent medium. The optical field $u(\mathbf{r}, L)$ is perpendicular to the propagation axis at $z = L$ km and is calculated with Huygens Fresnel integral as follows [63].

$$u(\mathbf{r}, L) = \frac{\exp(ikL)}{\lambda iL} \int_{-\infty}^{\infty} \int_{-\infty}^{\infty} \mathrm{d}^2\mathbf{s}\, u(\mathbf{s}, z = 0) \exp\left(\frac{ik}{2L} |\mathbf{s} - \mathbf{r}|^2 \right) \exp\left[\psi(\mathbf{s}, \mathbf{r}) \right], \tag{2.5}$$

where L is the path length, $i = \sqrt{-1}$, $z = L$ denotes the propagation axis, $u(\mathbf{s}, z = 0)$ is the optical wave at the source plane and $u(\mathbf{r}, L)$ is the optical field at the receiver plane, $\psi(\mathbf{s}, \mathbf{r})$ is the solution to Rytov method representing random part of the complex phase of a spherical wave propagating in the turbulence from the source point $(\mathbf{s}, z = 0)$ to the receiver point $(\mathbf{r}, L)$, $\mathbf{s} = (s_x, s_y)$ is transverse source coordinates and $\mathbf{r} = (r_x, r_y)$ is transverse receiver coordinates. It should be noted that Eq. (2.5) is utilized in the determination of many significant evaluations such as average intensity, mean field, scintillation, aperture averaging factor and <BER>. **r** coordinate at the receiver plane is transverse to the propagation axis.

2.4. BEAM INTENSITY AT RECEIVER PLANE IN UNDERWATER

The beam intensity at the receiver plane generated by the laser beam propagating in a turbulent environment is given by

$$I(\mathbf{r}, L) = u(\mathbf{r}, L) u^*(\mathbf{r}, L) \tag{2.6}$$

where * is the complex conjugate, thus $u^*(\mathbf{r}, L)$ is the conjugate of the field. Beam intensity is calculated by applying the extended Huygens Fresnel method. Using Eq. (2.5) and Eq. (2.6), instantaneous intensity at the receiver plane is found to be

$$I(\mathbf{r},L)=\frac{1}{(\lambda L)^2}\int_{-\infty}^{\infty}\int_{-\infty}^{\infty}\mathbf{d^2s_1}\int_{-\infty}^{\infty}\int_{-\infty}^{\infty}\mathbf{d^2s_2}u(\mathbf{s_1},z=0)u^*(\mathbf{s_2},z=0)\exp\left(\frac{ik}{2L}|\mathbf{s_1}-\mathbf{r}|^2\right)$$
$$\times\exp\left(-\frac{ik}{2L}|\mathbf{s_2}-\mathbf{r}|^2\right)\exp\left[\psi(\mathbf{s_1},\mathbf{r})\right]\exp\left[\psi^*(\mathbf{s_2},\mathbf{r})\right], \quad (2.7)$$

where

$$\begin{aligned}u(\mathbf{s_1},z=0)u^*(\mathbf{s_2},z=0)&=A\exp\left(-k\alpha|\mathbf{s_1}|^2\right)u_r(\mathbf{s_1},z=0)A^*\exp\left(-k\alpha^*|\mathbf{s_2}|^2\right)\\&=|A|^2\exp\left(-k\alpha|\mathbf{s_1}|^2\right)\exp\left(-k\alpha^*|\mathbf{s_2}|^2\right)\\&=|A|^2\exp\left(-k\alpha|\mathbf{s_1}|^2\right)\exp\left(-k\alpha^*|\mathbf{s_2}|^2\right). \quad (2.8)\end{aligned}$$

According to Eq. (2.7) and Eq. (2.8), the instantaneous intensity is

$$I(\mathbf{r},L)=\frac{1}{(\lambda L)^2}\int_{-\infty}^{\infty}\int_{-\infty}^{\infty}\mathbf{d^2s_1}\int_{-\infty}^{\infty}\int_{-\infty}^{\infty}\mathbf{d^2s_2}|A|^2\exp\left(-k\alpha|\mathbf{s_1}|^2\right)\exp\left(-k\alpha^*|\mathbf{s_2}|^2\right)$$
$$\times\exp\left(\frac{ik}{2L}|\mathbf{s_1}-\mathbf{r}|^2\right)\exp\left(-\frac{ik}{2L}|\mathbf{s_2}-\mathbf{r}|^2\right)\exp\left[\psi(\mathbf{s_1},\mathbf{r})\right]\exp\left[\psi^*(\mathbf{s_2},\mathbf{r})\right], \quad (2.9)$$

2.4.1. Average Intensity at the Receiver

The average intensity can be expressed as

$$\langle I(\mathbf{r},L)\rangle=\langle u(\mathbf{r},L)u^*(\mathbf{r},L)\rangle. \quad (2.10)$$

This equation also corresponds to the MCF or second order moment and the receiver coordinate is taken as $\mathbf{r_1}=\mathbf{r_2}=\mathbf{r}$ (identical observation points). Here $\langle\ \rangle$ represents the ensemble average over the turbulence statistics. The ensemble average is also called the mean or the expected value of the random process. Inserting Eq. (2.9) into Eq. (2.10), the average intensity becomes

$$\langle I(\mathbf{r},L)\rangle=\frac{1}{(\lambda L)^2}\int_{-\infty}^{\infty}\int_{-\infty}^{\infty}\mathbf{d^2s_1}\int_{-\infty}^{\infty}\int_{-\infty}^{\infty}\mathbf{d^2s_2}|A|^2\exp\left(-k\alpha|\mathbf{s_1}|^2\right)\exp\left(-k\alpha^*|\mathbf{s_2}|^2\right)$$
$$\times\exp\left(\frac{ik}{2L}|\mathbf{s_1}-\mathbf{r}|^2\right)\exp\left(-\frac{ik}{2L}|\mathbf{s_2}-\mathbf{r}|^2\right)$$
$$\times\langle\exp\left[\psi(\mathbf{s_1},\mathbf{r})\right]\exp\left[\psi^*(\mathbf{s_2},\mathbf{r})\right]\rangle. \quad (2.11)$$

The term $<\exp\left[\psi(\mathbf{s_1},\mathbf{r})\right]\exp\left[\psi^*(\mathbf{s_2},\mathbf{r})\right]>$ denotes the turbulence effect on the average intensity. Ensemble averaging over the turbulence statistics [69,158]

$$< \exp\left[\psi\left(\mathbf{s_1},\mathbf{r}\right)\right]\exp\left[\psi^*\left(\mathbf{s_2},\mathbf{r}\right)\right] > = \exp\left[-\frac{1}{2}D_\psi\left(\mathbf{s_1},\mathbf{s_2}\right)\right]$$

$$= \exp\left(-\frac{\left|\mathbf{s_1}-\mathbf{s_2}\right|^2}{\rho_0^2}\right), \tag{2.12}$$

where $D_\psi\left(\mathbf{s_1},\mathbf{s_2}\right)$ is the wave structure function, ρ_0 is the coherence length of a spherical wave propagating in the turbulent medium. In oceanic medium ρ_0 is known which is defined in Eq. (4.5) within the context of adaptive optics.

Inserting Eq. (2.12) in Eq. (2.11), the average intensity becomes

$$\langle I\left(\mathbf{r},L\right)\rangle = \frac{1}{\left(\lambda L\right)^2}\int_{-\infty}^{\infty}\int_{-\infty}^{\infty}\mathbf{d^2s_1}\int_{-\infty}^{\infty}\int_{-\infty}^{\infty}\mathbf{d^2s_2}\left|A\right|^2\exp\left(-k\alpha\left|\mathbf{s_1}\right|^2\right)\exp\left(-k\alpha^*\left|\mathbf{s_2}\right|^2\right)$$

$$\times\exp\left(\frac{ik}{2L}\left|\mathbf{s_1}-\mathbf{r}\right|^2\right)\exp\left(-\frac{ik}{2L}\left|\mathbf{s_2}-\mathbf{r}\right|^2\right)\exp\left(-\frac{\left|\mathbf{s_1}-\mathbf{s_2}\right|^2}{\rho_0^2}\right), \tag{2.13}$$

Expanding transverse coordinates into its components,

$$\langle I\left(\mathbf{r},L\right)\rangle = \frac{1}{\left(\lambda L\right)^2}\int_{-\infty}^{\infty}\int_{-\infty}^{\infty}\mathrm{d}s_{1x}\mathrm{d}s_{1y}\int_{-\infty}^{\infty}\int_{-\infty}^{\infty}\mathrm{d}s_{2x}\mathrm{d}s_{2y}\left|A\right|^2\exp\left(-k\alpha s_{1x}^2\right)\exp\left(-k\alpha s_{1y}^2\right)$$

$$\times\exp\left(-k\alpha^* s_{2x}^2\right)\exp\left(-k\alpha^* s_{2y}^2\right)$$

$$\times\exp\left\{-\frac{1}{\rho_0^2}\left[\left(s_{1x}-s_{2x}\right)^2+\left(s_{1y}-s_{2y}\right)^2\right]\right\}$$

$$\times\exp\left\{\frac{ik}{2L}\left[\left(s_{1x}-r_x\right)^2+\left(s_{1y}-r_y\right)^2\right]\right\}$$

$$\times\exp\left\{-\frac{ik}{2L}\left[\left(s_{2x}-r_x\right)^2+\left(s_{2y}-r_y\right)^2\right]\right\}, \tag{2.14}$$

Rearranging

$$\langle I\left(\mathbf{r},L\right)\rangle = \frac{1}{\left(\lambda L\right)^2}\int_{-\infty}^{\infty}\int_{-\infty}^{\infty}\mathrm{d}s_{1x}\mathrm{d}s_{1y}\int_{-\infty}^{\infty}\int_{-\infty}^{\infty}\mathrm{d}s_{2x}\mathrm{d}s_{2y}\left|A\right|^2\exp\left(-k\alpha s_{1x}^2\right)\exp\left(-k\alpha s_{1y}^2\right)$$

$$\times\exp\left(-k\alpha^* s_{2x}^2\right)\exp\left(-k\alpha^* s_{2y}^2\right)\exp\left\{-\frac{1}{\rho_0^2}\left(s_{1x}^2-2s_{1x}s_{2x}+s_{2x}^2+s_{1y}^2-2s_{1y}s_{2y}+s_{2y}^2\right)\right\}$$

$$\times\exp\left[\frac{ik}{2L}\left(s_{1x}^2-2s_{1x}r_x+r_x^2+s_{1y}^2-2s_{1y}r_y+r_y^2\right)\right]$$

$$\times\exp\left[-\frac{ik}{2L}\left(s_{2x}^2-2s_{2x}r_x+r_x^2+s_{2y}^2-2s_{2y}r_y+r_y^2\right)\right]. \tag{2.15}$$

Applying of the integration from Ref. [157]

$$\int_{-\infty}^{\infty} dx \exp\left(-t^2 x^2 \mp qx\right) = \pi^{0.5}/t \, \exp\left[q^2/4t^2\right], \qquad t>0 \tag{2.16}$$

Expressing the part of Eq. (2.11) for s_{1x} as

$$t_{1x}^2 = k\alpha + \frac{1}{\rho_0^2} - \frac{ik}{2L}, \; q_{1x} = \frac{2}{\rho_0^2} s_{2x} - \frac{ik}{L} r_x$$

Eq. (2.11) is converted to

$$\begin{aligned}\langle I(\mathbf{r}, L)\rangle = \frac{1}{(\lambda L)^2}\left(\pi^{0.5}/t_{1x}\right) \int_{-\infty}^{\infty} \mathrm{d}s_{1y} \int_{-\infty}^{\infty}\int_{-\infty}^{\infty} \mathrm{d}s_{2x}\mathrm{d}s_{2y} |A|^2 \exp\left[q_{1x}^2/\left(4t_{1x}^2\right)\right] \exp\left(-k\alpha s_{1y}^2\right) \\ \times \exp\left(-k\alpha^* s_{2x}^2\right) \exp\left(-k\alpha^* s_{2y}^2\right) \exp\left[-\frac{1}{\rho_0^2}\left(s_{2x}^2 + s_{1y}^2 - 2s_{1y}s_{2y} + s_{2y}^2\right)\right] \\ \times \exp\left[\frac{ik}{2L}\left(r_x^2 + s_{1y}^2 - 2s_{1y}r_y + r_y^2\right)\right] \\ \times \exp\left[-\frac{ik}{2L}\left(s_{2x}^2 - 2s_{2x}r_x + r_x^2 + s_{2y}^2 - 2s_{2y}r_y + r_y^2\right)\right].\end{aligned} \tag{2.17}$$

Substituting q_{1x} in Eq. (2.17)

$$\begin{aligned}\langle I(\mathbf{r}, L)\rangle = \frac{1}{(\lambda L)^2}\left(\pi^{0.5}/t_{1x}\right) \int_{-\infty}^{\infty} \mathrm{d}s_{1y} \int_{-\infty}^{\infty}\int_{-\infty}^{\infty} \mathrm{d}s_{2x}\mathrm{d}s_{2y} |A|^2 \exp\left\{\left[\frac{2}{\rho_0^2} s_{2x} - \frac{ik}{L} r_x\right]^2 / \left(4t_{1x}^2\right)\right\} \\ \times \exp\left(-k\alpha s_{1y}^2\right) \exp\left(-k\alpha^* s_{2x}^2\right) \exp\left(-k\alpha^* s_{2y}^2\right) \\ \times \exp\left\{-\frac{1}{\rho_0^2}\left(s_{2x}^2 + s_{1y}^2 - 2s_{1y}s_{2y} + s_{2y}^2\right)\right\} \\ \times \exp\left[\frac{ik}{2L}\left(r_x^2 + s_{1y}^2 - 2s_{1y}r_y + r_y^2\right)\right] \\ \times \exp\left[-\frac{ik}{2L}\left(s_{2x}^2 - 2s_{2x}r_x + r_x^2 + s_{2y}^2 - 2s_{2y}r_y + r_y^2\right)\right],\end{aligned} \tag{2.18}$$

By expanding the Eq.(2.18), Eq.(2.19) is obtained.

$$\langle I(\mathbf{r},L)\rangle = \frac{1}{(\lambda L)^2}\left(\pi^{0.5}/t_{1x}\right)\int_{-\infty}^{\infty} ds_{1y}\int_{-\infty}^{\infty}\int_{-\infty}^{\infty} ds_{2x}ds_{2y}|A|^2 \exp\left\{\frac{1}{t_{1x}^2}\left(\frac{1}{\rho_0^2}\right)^2 s_{2x}^2 - \frac{ik}{t_{1x}^2 L}\frac{1}{\rho_0^2}s_{2x}r_x - \frac{k^2}{4t_{1x}^2L^2}r_x^2\right\}$$
$$\times\exp\left(-k\alpha s_{1y}^2\right)\exp\left(-k\alpha^* s_{2x}^2\right)\exp\left(-k\alpha^* s_{2y}^2\right)$$
$$\times\exp\left\{-\frac{1}{\rho_0^2}\left(s_{2x}^2+s_{1y}^2-2s_{1y}s_{2y}+s_{2y}^2\right)\right\}$$
$$\times\exp\left[\frac{ik}{2L}\left(r_x^2+s_{1y}^2-2s_{1y}r_y+r_y^2\right)\right]$$
$$\times\exp\left[-\frac{ik}{2L}\left(s_{2x}^2-2s_{2x}r_x+r_x^2+s_{2y}^2-2s_{2y}r_y+r_y^2\right)\right]. \qquad (2.19)$$

For s_{2x}, defining

$t_{2x}^2 = k\alpha^* + \frac{1}{\rho_0^2} + \frac{ik}{2L} - \frac{1}{t_{1x}^2}\left(\frac{1}{\rho_0^2}\right)^2$, $q_{2x} = \frac{ik}{L}r_x - \frac{ik}{t_{1x}^2 L}\frac{1}{\rho_0^2}r_x$ and integrating over s_{2x}

$$\langle I(\mathbf{r},L)\rangle = \frac{1}{(\lambda L)^2}\left(\pi^{0.5}/t_{1x}\right)\left(\pi^{0.5}/t_{2x}\right)$$
$$\times\exp\left[q_{2x}^2/\left(4t_{2x}^2\right)\right]\int_{-\infty}^{\infty} ds_{1y}\int_{-\infty}^{\infty} ds_{2y}|A|^2\exp\left\{-\frac{k^2}{4t_{1x}^2L^2}r_x^2\right\}$$
$$\times\exp\left(-k\alpha s_{1y}^2\right)\exp\left(-k\alpha^* s_{2y}^2\right)\exp\left\{-\frac{1}{\rho_0^2}\left(s_{1y}^2-2s_{1y}s_{2y}+s_{2y}^2\right)\right\}$$
$$\times\exp\left[\frac{ik}{2L}\left(r_x^2+s_{1y}^2-2s_{1y}r_y+r_y^2\right)\right]\exp\left[-\frac{ik}{2L}\left(r_x^2+s_{2y}^2-2s_{2y}r_y+r_y^2\right)\right], \qquad (2.20)$$

Since the integration for *y* components of the integral is exactly the same as the integration for *x* components, except r_x is replaced by r_y, when integrated over s_{1y} and s_{2y}, Eq. (2.20) becomes

$$\langle I(\mathbf{r},L)\rangle = \frac{|A|^2\pi^2}{(\lambda L)^2 t_{1x}^2 t_{2x}^2}\exp\left(0.25q_{2x}^2/t_{2x}^2\right)$$
$$\times\exp\left(0.25q_{2y}^2/t_{2y}^2\right)\exp\left(-\frac{k^2}{4t_{1x}^2L^2}r_x^2\right)\exp\left(-\frac{k^2}{4t_{1y}^2L^2}r_y^2\right), \qquad (2.21)$$

where, $t_{1y}^2 = t_{1x}^2 = k\alpha + \frac{1}{\rho_0^2} - \frac{ik}{2L}$, $t_{2y}^2 = t_{2x}^2 = k\alpha^* + \frac{1}{\rho_0^2} + \frac{ik}{2L} - \frac{1}{t_{1x}^2}\left(\frac{1}{\rho_0^2}\right)^2$, and

$q_{2y} = \frac{ik}{L}r_y - \frac{ik}{t_{1y}^2 L}\frac{1}{\rho_0^2}r_y$

t_{1x}^2 and t_{1y}^2 can be denoted as t_1^2 , t_{2x}^2 and t_{2y}^2 as t_2^2.

$$t_{1x}^2 = t_{1y}^2 = t_1^2 = ka + \frac{1}{\rho_0^2} - \frac{ik}{2L},\ t_{2x}^2 = t_{2y}^2 = t_2^2 = ka^* + \frac{1}{\rho_0^2} + \frac{ik}{2L} - \frac{1}{t_1^2\rho_0^4}$$

The conjugate of Eq. (2.4) is

$$\alpha^* = \frac{1}{2k\alpha_s^2} - \frac{i}{2F} \tag{2.22}$$

Focal length is set to $F \to \infty$ (collimated beam) so,

$$\alpha = \alpha^* = \frac{1}{2k\alpha_s^2}, \tag{2.23}$$

where, $t_1^2 = k\left(\frac{1}{2k\alpha_s^2}\right) + \frac{1}{\rho_0^2} - \frac{ik}{2L},\ t_2^2 = k\left(\frac{1}{2k\alpha_s^2}\right) + \frac{1}{\rho_0^2} + \frac{ik}{2L} - \frac{1}{t_1^2\rho_0^4},$

$q_{2x} = \frac{ik}{L}r_x - \frac{ik}{t_1^2 L}\frac{1}{\rho_0^2}r_x,\ q_{2y} = \frac{ik}{L}r_y - \frac{ik}{t_1^2 L}\frac{1}{\rho_0^2}r_y.$

Finally, Eq. (2.24) is found to be

$$\langle I(\mathbf{r},L)\rangle = \frac{|A|^2\pi^2}{(\lambda L)^2 t_1^2 t_2^2}\exp\left(\frac{q_{2x}^2 + q_{2y}^2}{4t_2^2}\right)\exp\left(-\frac{k^2}{4t_1^2L^2}(r_x^2 + r_y^2)\right) \tag{2.24}$$

Substituting t_1^2, t_2^2, q_{2x} and q_{2y} in Eq.(2.24) and showing in the complete form

$$\langle I(\mathbf{r},L)\rangle = \frac{\pi^2}{(\lambda L)^2}\frac{|A|^2}{\left(k\alpha+\frac{1}{\rho_0^2}-\frac{ik}{2L}\right)\left[k\alpha^*+\frac{1}{\rho_0^2}+\frac{ik}{2L}-\frac{1}{\left(k\alpha+\frac{1}{\rho_0^2}-\frac{ik}{2L}\right)\rho_0^4}\right]}\exp\left\{\frac{-k^2\left(k\alpha+k\alpha^*\right)\left(r_x^2+r_y^2\right)}{4L^2\left(k\alpha+\frac{1}{\rho_0^2}-\frac{ik}{2L}\right)\left[k\alpha^*+\frac{1}{\rho_0^2}+\frac{ik}{2L}-\frac{1}{\left(k\alpha+\frac{1}{\rho_0^2}-\frac{ik}{2L}\right)\rho_0^4}\right]}\right\} \tag{2.25}$$

$$\langle I(\mathbf{r},L)\rangle = \frac{\pi^2}{(\lambda L)^2}\frac{|A|^2}{\left(k\alpha+\frac{1}{\rho_0^2}-\frac{ik}{2L}\right)\left(k\alpha^*+\frac{1}{\rho_0^2}+\frac{ik}{2L}\right)-\left(\frac{1}{\rho_0^4}\right)}\exp\left[\frac{-k^2\left(k\alpha+k\alpha^*\right)\left(r_x^2+r_y^2\right)}{4L^2\left(k\alpha+\frac{1}{\rho_0^2}-\frac{ik}{2L}\right)\left(k\alpha^*+\frac{1}{\rho_0^2}+\frac{ik}{2L}\right)-\left(\frac{1}{\rho_0^4}\right)}\right] \tag{2.26}$$

$$\langle I(\mathbf{r},L)\rangle = \frac{\pi^2}{(\lambda L)^2}\frac{|A|^2}{\left(\frac{1}{2\alpha_s^2}+\frac{1}{\rho_0^2}-\frac{ik}{2L}\right)\left(\frac{1}{2\alpha_s^2}+\frac{1}{\rho_0^2}+\frac{ik}{2L}\right)-\left(\frac{1}{\rho_0^4}\right)}\exp\left[\frac{-k^2\left(\frac{1}{2\alpha_s^2}+\frac{1}{2\alpha_s^2}\right)\left(r_x^2+r_y^2\right)}{4L^2\left(\frac{1}{2\alpha_s^2}+\frac{1}{\rho_0^2}-\frac{ik}{2L}\right)\left(\frac{1}{2\alpha_s^2}+\frac{1}{\rho_0^2}+\frac{ik}{2L}\right)-\left(\frac{1}{\rho_0^4}\right)}\right] \tag{2.27}$$

To see Eq. (2.27) more clearly, defining

$$t_1 = \frac{k^2 y_1}{4L^2 x_1},\ \ y_1 = \frac{1}{\alpha_s^2},\ x_1 = ab - c \ \text{ and } \alpha = \frac{1}{2\alpha_s^2} + \frac{1}{\rho_0^2} - \frac{ik}{2L},\ b = \frac{1}{2\alpha_s^2} + \frac{1}{\rho_0^2} + \frac{ik}{2L},\ c = \frac{1}{\rho_0^4},$$

then the average intensity was obtained

$$\langle I(\mathbf{r}, L)\rangle = \frac{\pi^2}{(\lambda L)^2}\frac{|A|^2}{ab-c}\exp\left[\frac{-k^2 y_1\left(r_x^2 + r_y^2\right)}{4L^2(ab-c)}\right] \tag{2.28}$$

which is

$$\langle I(\mathbf{r}, L)\rangle = \frac{\pi^2}{(\lambda L)^2}\frac{|A|^2}{x_1}\exp\left[\frac{-k^2 y_1\left(r_x^2 + r_y^2\right)}{4L^2 x_1}\right], \tag{2.29}$$

and finally

$$\langle I(\mathbf{r}, L)\rangle = \frac{\pi^2}{(\lambda L)^2}\frac{|A|^2}{x_1}\exp\left[-t_1\left(r_x^2 + r_y^2\right)\right] \tag{2.30}$$

CHAPTER 3

BEAM SIZE AND BEAM SPREAD

3.1. METHODOLOGY OF THE BEAM SIZE AND BEAM SPREAD

In this thesis, the effect of adaptive optic filters on the beam size and the beam spread has been studied. The main purpose of this thesis is to obtain beam spread and the beam size values for each adaptive optics filtered and unfiltered cases and to demonstrate the beneficial effect of AOF method in communication systems. This part starts with Carter's formula that provides the definition of the beam size in the r_x direction.

The beam size or the effective beam spot was expressed through Carter's formula as [68]

$$\sigma_{xL} = \sqrt{\frac{2\int_{-\infty}^{\infty}\int_{-\infty}^{\infty} r_x^2 \langle I(r_x, r_y, L)\rangle dr_x dr_y}{\int_{-\infty}^{\infty}\int_{-\infty}^{\infty} \langle I(r_x, r_y, L)\rangle dr_x dr_y}}, \tag{3.1}$$

$$\sigma_{xL} = \sqrt{\frac{2\int_{-\infty}^{\infty}\int_{-\infty}^{\infty} r_x^2 \langle I(r_x, r_y, L)\rangle dr_x dr_y}{\int_{-\infty}^{\infty}\int_{-\infty}^{\infty} \langle I(r_x, r_y, L)\rangle dr_x dr_y}} = \sqrt{\frac{A}{B}}, \tag{3.2}$$

where $\langle I(r_x, r_y, L)\rangle$ is the average intensity and r_x and $r_{y,}$ is the transverse coordinate at the receiver. When the variable is changed to solve in two parts, Eq. (3.1) can be written as Eq. (3.2) by defining A and B as

$$A = 2\int_{-\infty}^{\infty}\int_{-\infty}^{\infty} r_x^2 \langle I(r_x, r_y, L)\rangle dr_x dr_y \tag{3.3}$$

$$B = \int_{-\infty}^{\infty}\int_{-\infty}^{\infty} \langle I(r_x, r_y, L)\rangle dr_x dr_y \tag{3.4}$$

Using Eq. (2.30), Eq. (3.3) and Eq. (3.4) are converted to Eq. (3.5) and Eq. (3.6), respectively as

$$A = 2\frac{\pi^2}{(\lambda L)^2}\frac{|A|^2}{x_1}\int_{-\infty}^{\infty}\int_{-\infty}^{\infty} r_x^2 dr_x dr_y \exp\left[-t_1\left(r_x^2 + r_y^2\right)\right], \tag{3.5}$$

$$B = \frac{\pi^2}{(\lambda L)^2}\frac{|A|^2}{x_1}\int_{-\infty}^{\infty}\int_{-\infty}^{\infty} dr_x dr_y \exp\left[-t_1\left(r_x^2 + r_y^2\right)\right]. \tag{3.6}$$

With the application of the integration from Ref. [157], the integrals for B and second part of the integral for A can be solved. Applying the integral in [157] to the second integral of A and both integrals of B.

$$\int_{-\infty}^{\infty} \exp\left(-t_1 r_x{}^2 + q r_x\right) dr_x \text{ and } \int_{-\infty}^{\infty} \exp\left(-t_1 r_y{}^2 + q r_y\right) dr_y = \exp\left(\tfrac{q^2}{4t_1}\right) \tfrac{\sqrt{\pi}}{\sqrt{t_1}},$$

$$q = 0 \Rightarrow \tfrac{\sqrt{\pi}}{\sqrt{t_1}} \to t_1 > 0 \tag{3.7}$$

Also the other integration is the first integral of A in Eq. (3.5) which is

$$\int_{-\infty}^{\infty} r_x{}^2 \exp\left(-t_1 r_x{}^2 + q r_x\right) dr_x. \tag{3.8}$$

To solve Eq. (3.8) we apply Ryzhik [157] and obtain

$$\int_{-\infty}^{\infty} x^2 \exp\left(-\mu x^2 + 2\nu x\right) dx = \tfrac{1}{2\mu} \sqrt{\tfrac{\pi}{\mu}\left(1 + 2\tfrac{\nu^2}{\mu}\right)} \exp\left(\tfrac{\nu^2}{\mu}\right),$$

$$\nu = 0 \Rightarrow \int_{-\infty}^{\infty} x^2 \exp\left(-\mu x^2\right) dx = \tfrac{1}{2\mu} \sqrt{\tfrac{\pi}{\mu}},$$

$$\int_{-\infty}^{\infty} r_x{}^2 \exp\left(-t_1 r_x{}^2\right) dr_x = \tfrac{1}{2t_1} \sqrt{\tfrac{\pi}{t_1}} \tag{3.9}$$

If A and B are inserted in Eq. (3.2), the beam size throughout the propagation axis is obtained to be

$$\sigma_{xL} = \sqrt{\frac{2\frac{\pi^2}{(\lambda L)^2}\frac{|A|^2}{x_1}\left(\frac{1}{2t_1}\sqrt{\frac{\pi}{t_1}}\right)\left(\sqrt{\frac{\pi}{t_1}}\right)}{\frac{\pi^2}{(\lambda L)^2}\frac{|A|^2}{x_1}\left(\sqrt{\frac{\pi}{t_1}}\right)\left(\sqrt{\frac{\pi}{t_1}}\right)}} = \sqrt{\frac{\frac{\pi}{x_1 t_1^2}}{\frac{\pi}{x_1 t_1}}} = \sqrt{\frac{1}{t_1}} \tag{3.10}$$

To observe the beam spread that shows the turbulence effect on the beam size, beam size in the absence of turbulence (i.e., free space) is subtracted from the beam size in the presence of turbulence, which is expressed as

$$\triangle\sigma_{xL} = \sigma_{xL\_oc}\left(z = L\right) - \sigma_{xL\_fs}\left(z = L\right), \tag{3.11}$$

When beam size in r_x direction at receiver plane after the beam propagates in underwater turbulent medium it is expressed as $\sigma_{xL\_oc}\left(z = L\right)$, and when beam size in r_x direction at receiver plane after the beam propagates in the absence of turbulence (namely in free space) it is expressed as $\sigma_{xL\_fs}\left(z = L\right)$.

CHAPTER 4

ADAPTIVE OPTICS CORRECTIONS

4.1. METHODOLOGY OF THE ADAPTIVE OPTICS CORRECTIONS

AO corrections were applied to mitigate the detrimental effects of turbulence on light beam propagation. There are a variety of different designs of AO systems, but they all have similar logic to reduce the detrimental effect of turbulence. In this thesis, useful effects of the AO method on the system were investigated. Adaptive optics corrections such as piston, focus, tilt, astigmatism impacts, and the sum of they are analyzed against the underwater turbulence parameters for different wavelengths, link lengths and source sizes. AO techniques are among the best methods to reduce the turbulence-caused optical degradation of the beam [149].

The adaptive optics filter function is used in adaptive optics method [155,156].

$$1-\sum_{l=1}^{N} F_l(\kappa, D, \theta) \tag{4.1}$$

where $F_l(\kappa, D, \theta)$ is the filter function consisting of sinusoidal functions and Bessel. It was expressed for $m=0$ by

$$F_{m=0,n}(\kappa, D, \theta) = (n+1)\left[\frac{2J_{n+1}(0.5\kappa D)}{0.5\kappa D}\right]^2, \tag{4.2}$$

for even m by

$$F_{m=even,n}\left(\kappa, D, \theta\right) = 2\left(n+1\right)\left[\frac{2J_{n+1}\left(0.5\kappa D\right)}{0.5\kappa D}\right]^2 \cos^2\left(m\theta\right), \tag{4.3}$$

and for odd m by

$$F_{m=odd,n}\left(\kappa, D, \theta\right) = 2\left(n+1\right)\left[\frac{2J_{n+1}\left(0.5\kappa D\right)}{0.5\kappa D}\right]^2 \sin^2\left(m\theta\right) \tag{4.4}$$

where $\kappa = (\kappa, \theta)$ is the spatial frequency vector in polar coordinates and $\kappa = |\kappa|$ represents the amplitude of the spatial frequency, D is the receiver aperture diameter, J is the Bessel function of the first kind and. (m=0, n=0), (m=1, n=1), (m=2, n=2) and (m=0, n=2) denote the piston, tilt, astigmatism and focus (defocus), respectively. In Eq. (4.1), N represents the number of correction terms taken in the overall AO correction. N = 1 is expressed when only the tilt component or only the piston component is used, N = 2 when both the piston and tilt components are used, and N = 3 when the piston, tilt, and astigmatism components are used. ρ_0 is the spatial coherence length of a spherical wave propagating in the turbulent medium and ρ_0 in Eq. (2.12) when θ integration is executed, is expressed as [158]

$$\rho_0 = \left[\frac{1}{3} \pi^2 k^2 z \int_0^\infty \kappa^3 \Phi_n(\kappa) d\kappa \right]^{-0.5}. \tag{4.5}$$

In polar coordinates Eq. (4.5) is expressed as

$$\rho_0 = \left[\frac{1}{6} \pi^2 k^2 z \int_0^\infty \int_0^{2\pi} \kappa^3 \Phi_n(\kappa) d\theta d\kappa \right]^{-0.5} \tag{4.6}$$

is found with numerical integration using MATLAB. Kappa integral is from zero to infinity but we took it from $\frac{2\pi}{25\text{ m}}$ to $\frac{2\pi}{1\text{ mm}}$ because outer scale is 25 m and the inner scale is 1 mm.

When adaptive optics is not considerd, the coherence length of the underwater medium is given as [158]

$$\rho_0 = \left[3.603 \times 10^{-7} k^2 z \frac{(\varepsilon\eta)^{-1/3} X_{\mathrm{T}}}{2\omega^2} \left(0.483\omega^2 - 0.835\omega + 3.38 \right) \right]^{-0.5} \tag{4.7}$$

To find the coherence length in Eq. (4.6), spectrum of the oceanic turbulence should be rearrangered according to the applied AO corrections. $\Phi_n(\kappa)$ given in Eq. (2.2) is modified by the adaptive optics filter function given by Eq. (4.1) to obtain the modified spectrum of the oceanic turbulence to be

$$\Phi_n(\kappa) = 0.388 C_m^2 \omega^{-2} \kappa^{-11/3} \left[1 + 2.35(\kappa\eta)^{2/3} \right] (\omega^2 e^{-A_T \delta} + e^{-A_S \delta} - 2\omega e^{-A_{TS} \delta}) \times \left\{ \left[1 - \sum_{l=1}^{N} F_l(\kappa, D, \theta) \right] \right\}. \tag{4.8}$$

Eq. (4.8) is used in Eq. (4.6) to find ρ_0 which in turn is employed in Eq. (3.10) and Eq. (3.11) to find the beam spread.

CHAPTER 5

NUMERICAL RESULTS

In Figure 1, the graphs show the beam size with no adaptive optics, only focus corrected (F only), only astigmatism corrected (A only), only tilt corrected (T only), only piston corrected (P only), and the sum of tilt, focus, astigmatism and piston corrected (T+F+A+P). When χ_T increases, effects of oceanic turbulence increase. This increase in turbulence strength makes the beam size bigger. It is also depicted from Figure 1 that for all χ_T, the beam size is the largest for with no AO, and the beam size becomes smaller is for A only, F only (the same as A only), T only, P only and it gets the smallest for the sum of corrections (T+F+A+P).

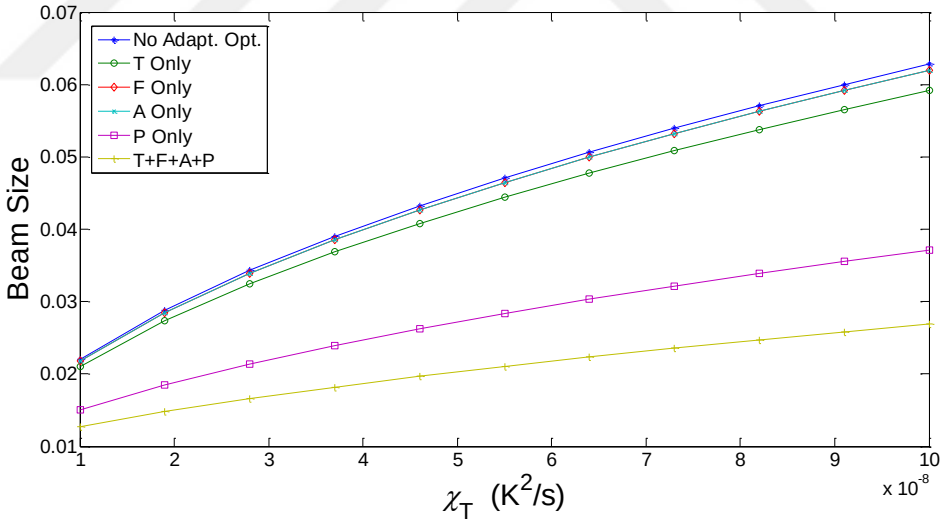

Figure 1: The beam size against χ_T at various adaptive optics and with no adaptive optics.

It is seen in Figure 2 that if ω is close to zero (i.e. salinity-based turbulence), the effect of the turbulence increases and the beam size increases. Also, for a fixed ω, the beam size at the receiver plane is the smallest when the sum of all the corrections is applied.

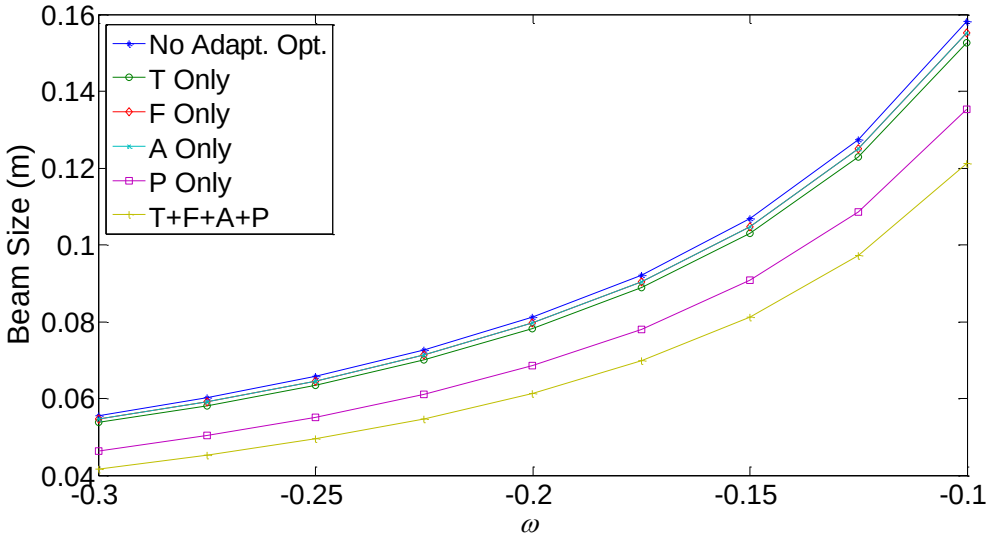

Figure 2: The The beam size against ω at various adaptive optics and with no adaptive optics.

Figure 3 has the opposite trend when compared to Figure 1 and Figure 2. Namely, as ε increases, the beam size decreases. As ε increases, the strength of the oceanic turbulence decreases. In terms of applying AOF, the same trend as in Figures 1 and 3 is observed. It is also seen from Figure 3 that when ε is kept at a fixed value, the beam size is the largest for without AO correction, and the value of the beam size becoming smaller is for A only, F only (the same as A only), T only, P only and the smallest beam size value is obtained for the sum of all corrections (T+F+A+P).

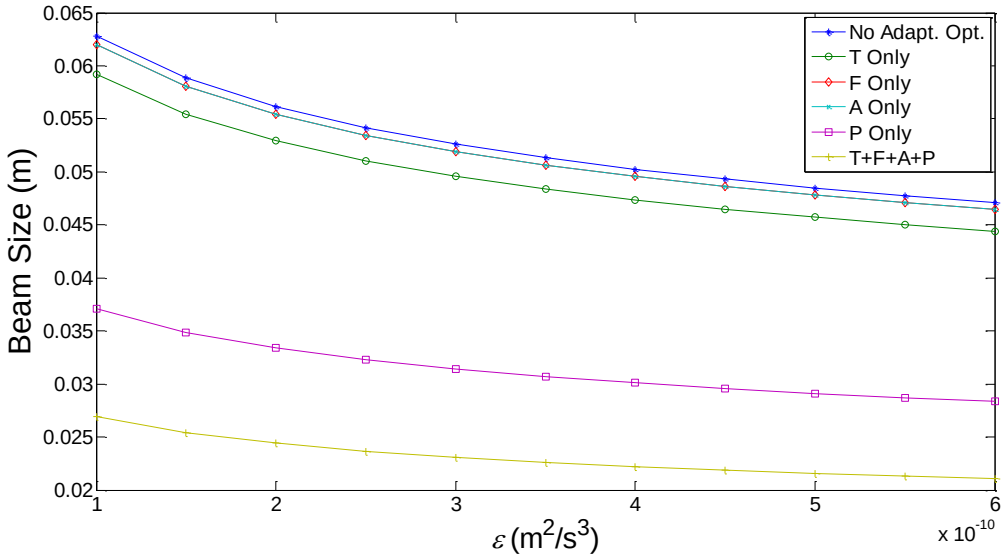

Figure 3: The beam size against ε at various adaptive optics and with no adaptive optics.

In Figure 4, we can make the same inferences as in Figure 2. It can be seen that as the ω value increases, the beam size becomes larger and the sum of the AOF

decreases the beam size. Figure 4 also shows that at fixed χ_T value, as ω increases the difference between the beam size values for the sum of the adaptive optical filters and without adaptive optical correction become larger. Also in Figure 4, the difference between the beam size for adaptive optics and the beam size for the correction sum increases as χ_T increases.

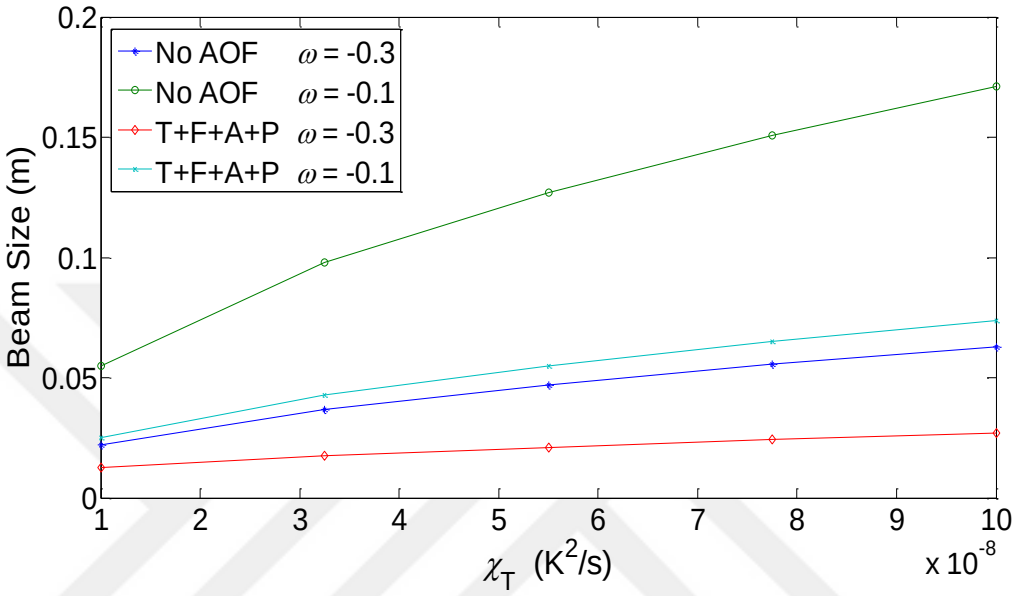

Figure 4: The beam size against χ_T at various ω that use adaptive optics and use with no adaptive optics.

Figure 5 shows that as the source size increases, beam size increases. Also, it can be said that the turbulence effect increases when χ_T increases and the adaptive optics correction becomes more effective for large χ_T value. If we compare the curves without AO correction with the curves with the sum of the AO correction for $\alpha_s = 0.01$ and for $\alpha_s = 0.15$, we can deduce that adaptive optics correction is more effective at small α_s values.

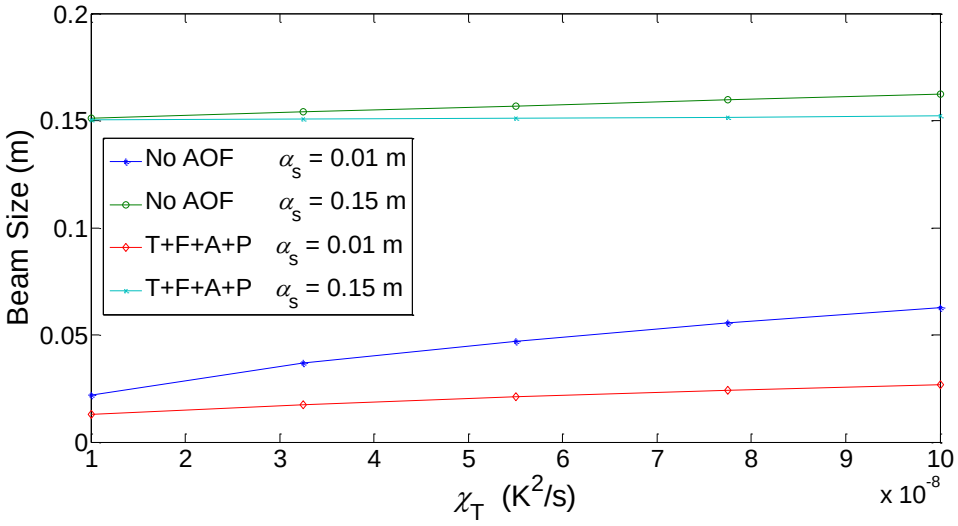

Figure 5: The beam size against χ_T at various α_s values that use adaptive optics and use with no adaptive optics.

Figure 6 trend is similar to Figure 5 because as χ_T and ω increase, beam size value increases. As in Figure 5, the difference between without adaptive optics curve and sum of adaptive optics curve for α_s = 0.01 is greater than the difference for α_s = 0.15 in Figure 6, so it can be deduced that the effectiveness of adaptive optics correction increases as α_s decreases. Another inference is that with increasing salinity, in other words, with more turbulence, the effect of the adaptive optical filter increases.

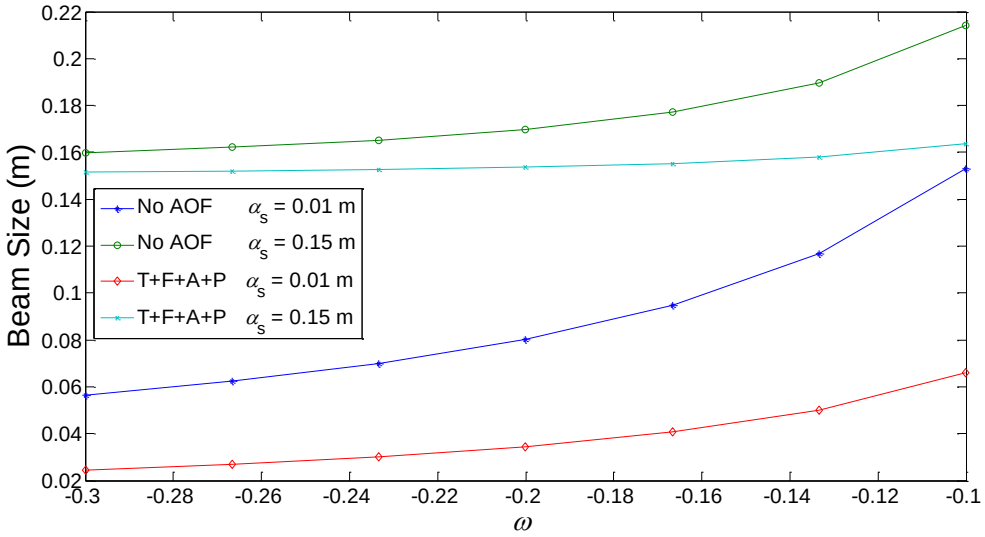

Figure 6: The beam size against ω at various α_s values that use adaptive optics and use with no adaptive optics.

Since the turbulence strength and ε are inversely proportional, the increase in ε causes the beam size to decrease, so the curves in Figure 7 show the opposite trend of the curves in Figures 5 and 6. The adaptive optics filter can show its effect more when turbulence strength is high, so the effect of the filter increases with decreasing ε in Figure 7. The common deduction of Figures 5-7 is that with decreasing α_s, beam size decreases, and for small α_s the sum adaptive optics filter becomes more effective.

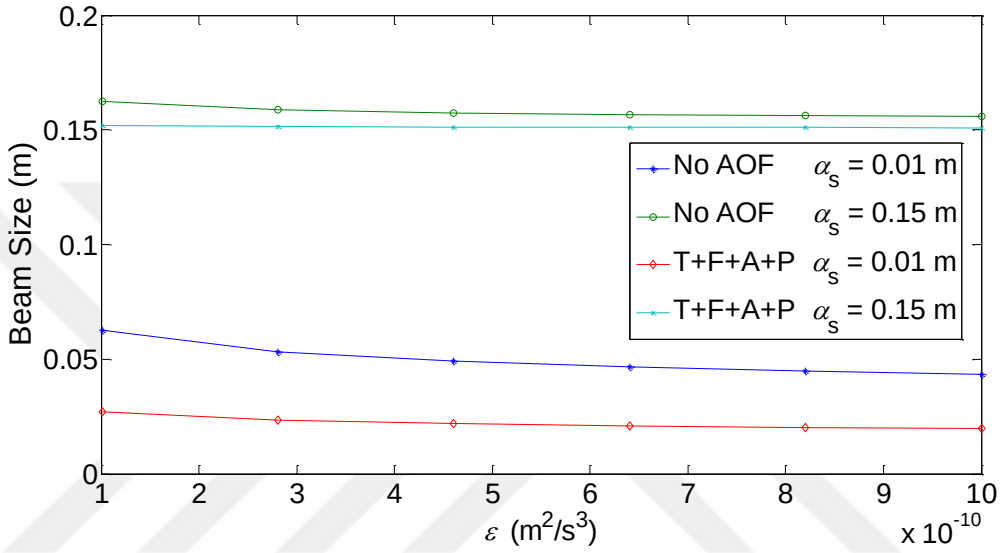

Figure 7: The beam size against ε at various α_s values that use adaptive optics and use with no adaptive optics.

Figure 8 shows that the beam size against χ_T at various receiver aperture diameter values that use T+F+A+P and use with no adaptive optics. Figure 8 shows that for a fixed D, larger χ_T results in larger beam size. Figure 8 shows that at any χ_T, smaller receiver aperture diameter ends up with smaller beam size and T+F+A+P correction at smaller receiver diameter is more effective for all value of χ_T.

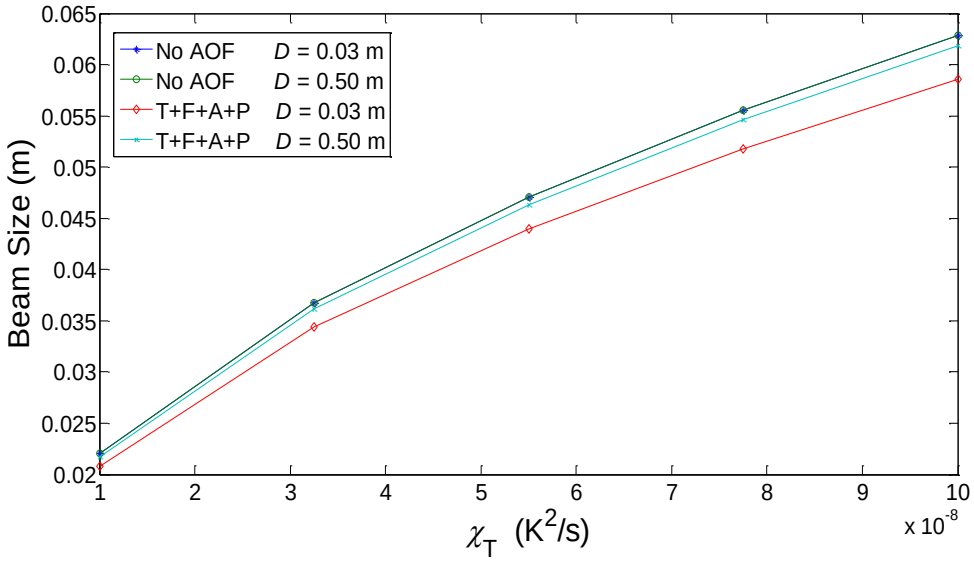

Figure 8: The beam size against χ_T at various D values that use adaptive optics and use with no adaptive optics.

Figure 9 reflects the beam size at T+F+A+P AO correction against ω at various D values. Figure 9 shows that for all the D values, larger ω causes larger beam size. Another result is that for a constant ω, smaller D value yields smaller beam size and T+F+A+P correction at smaller receiver diameter is most effective.

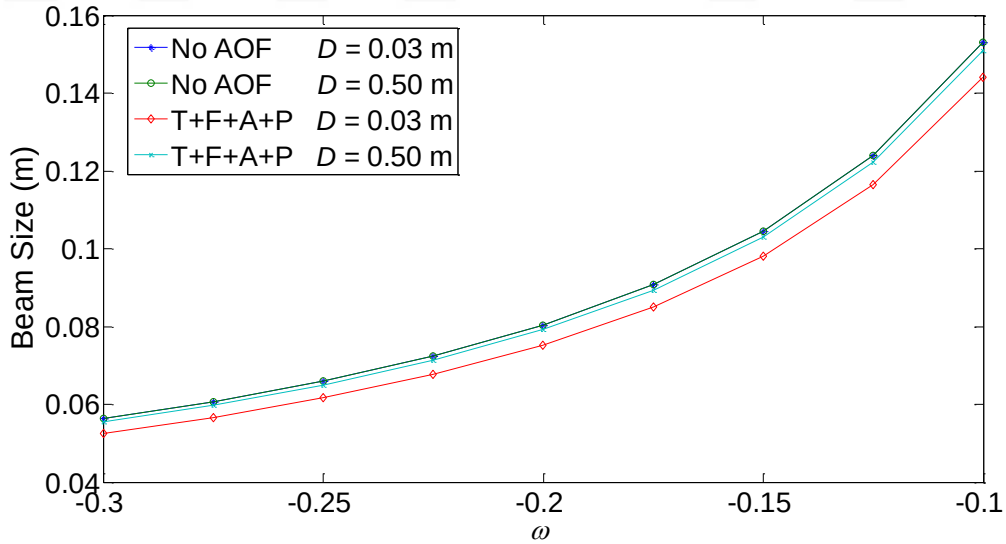

Figure 9: The beam size against ω at various D values that use adaptive optics and use with no adaptive optics.

Figure 10 shows the beam size using without and using with no adaptive optics against ε for various D values. It is seen that for any D, smaller ε yields

larger beam size and T+F+A+P correction for smaller D is most effective at every ε value.

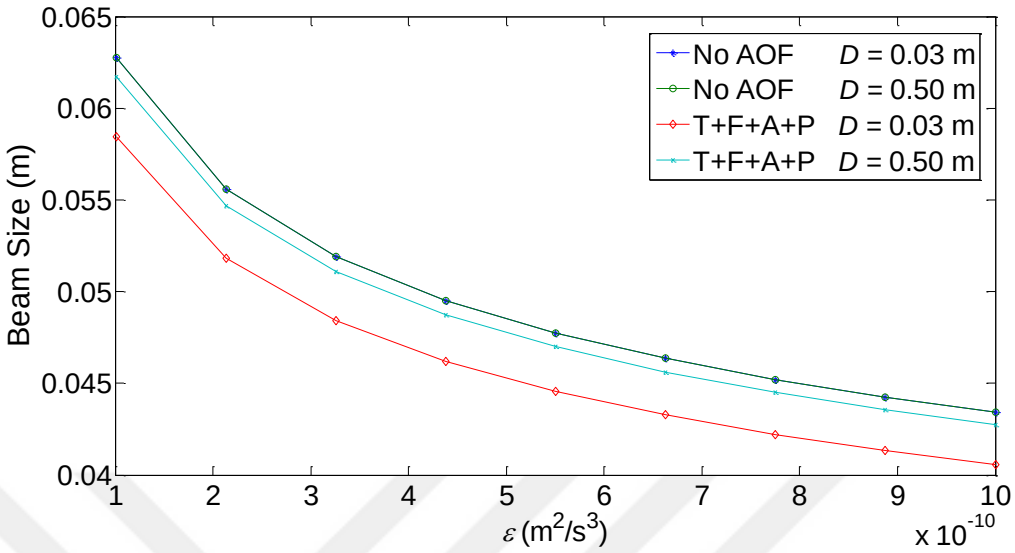

Figure 10: The beam size against ε at various D values that use adaptive optics and use with no adaptive optics.

Figure 11 shows the beam size at T+F+A+P adaptive optics correction versus χ_T for different inner scale of the turbulence in oceanic turbulence. Increasing χ_T causes an increase in the beam size value. In Figure 11, it is observed that at any χ_T, larger inner scale yields a decrease in the beam size, so it can be deduced that the effect of T+F+A+P correction increases with the increase of the inner scale value.

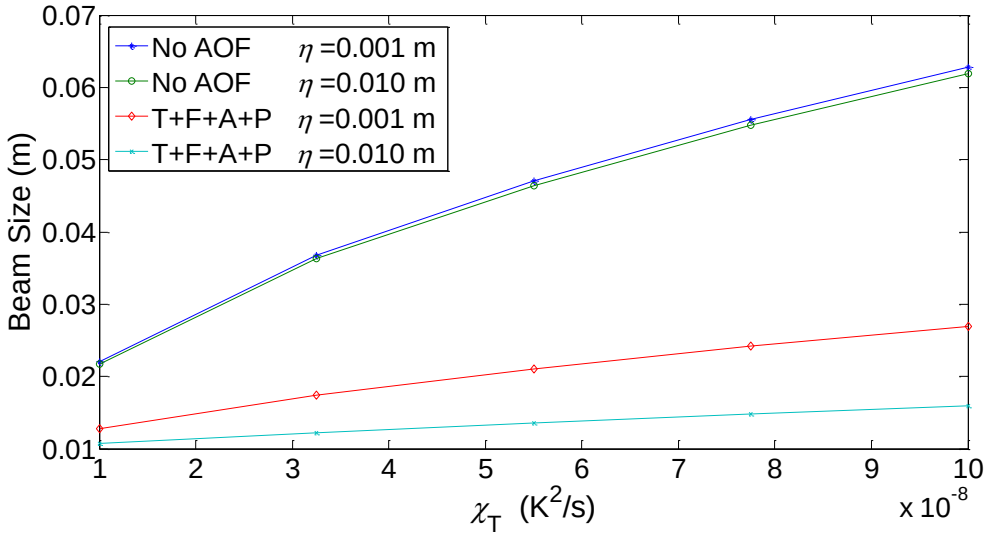

Figure 11: The beam size against χ_T at various inner scale values that use adaptive optics and use with no adaptive optics.

In can be seen in Figure 12 that T+F+A+P correction is more effective for larger inner scale value. Also, with increasing ω, beam size increases and the effectiveness of T+F+A+P correction also increases.

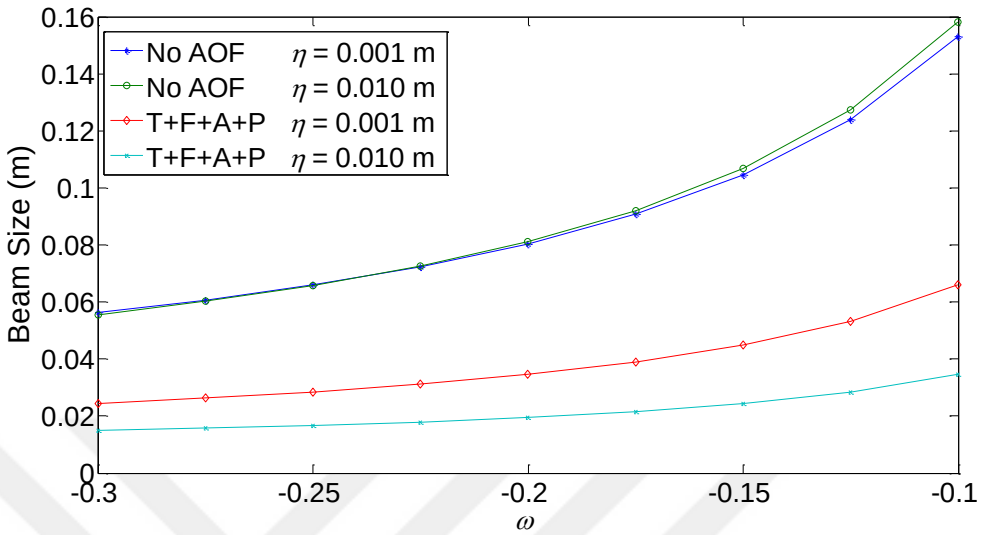

Figure 12: The beam size against ω at various inner scale values that use adaptive optics and use with no adaptive optics.

Figure 13 shows the beam size at T+F+A+P AO correction against ε at various inner scale values. The observation is that smaller ε causes the beam size to increase. Figure 13 also shows that at any ε, larger inner scale value yields a decrease in the beam size so it can be deduced that the effect of T+F+A+P correction increases with the increase of the inner scale value.

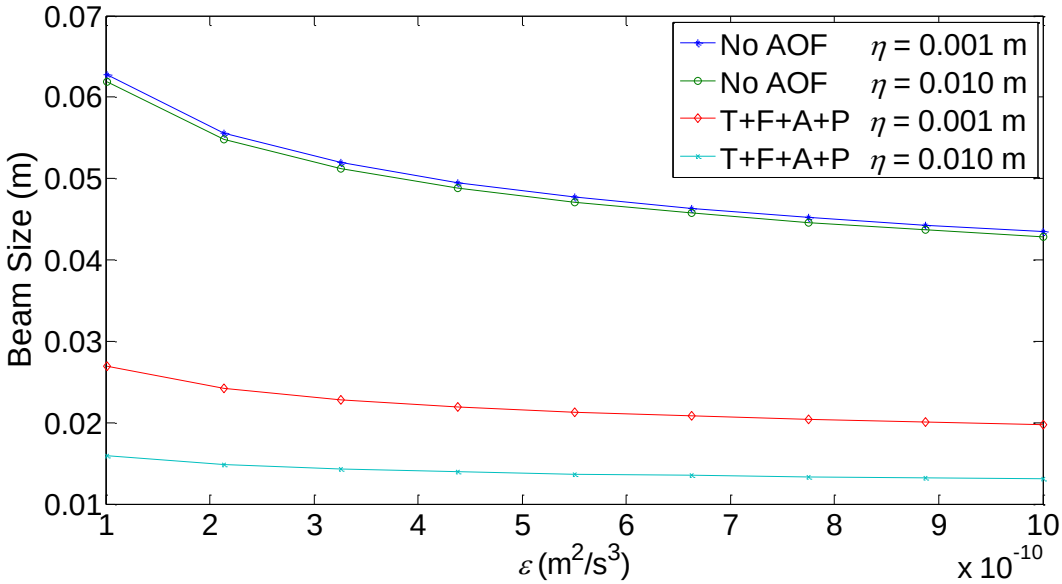

Figure 13: The beam size against ε at various inner scale values that use adaptive optics and use with no adaptive optics.

Figure 14 is shows the beam size using without and with AO correction against χ_T at various link length values. Also, for all χ_T values, larger link length results in larger beam size, namely at a fixed χ_T, the AO corrected beam size value is also larger at larger link lengths. Other result in Figure 14 is that the reduction percentages of the beam sizes at various link lengths are the same at all χ_T. The reduction of the beam size is larger at the larger link length.

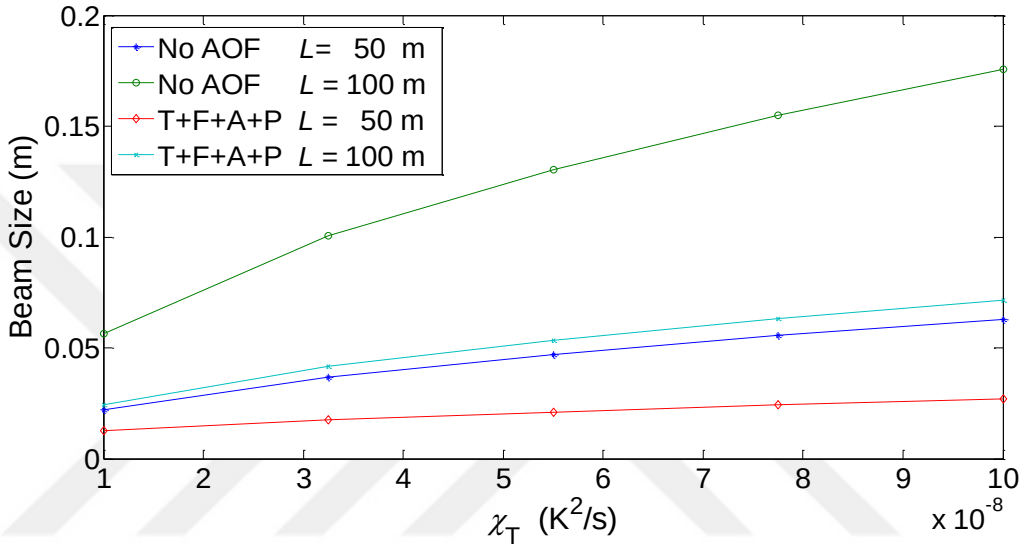

Figure 14: The beam size against χ_T at various link lengths that use adaptive optics and use with no adaptive optics.

Figure 15 shows the beam size at T+F+A+P adaptive optics correction versus ω for various link lengths. Increasing ω causes an increase in the beam size value. In Figure 15, it is observed that at any ω, larger link length yields an increase in the beam size so it can be deduced that the effect of T+F+A+P correction increases with increasing the link length.

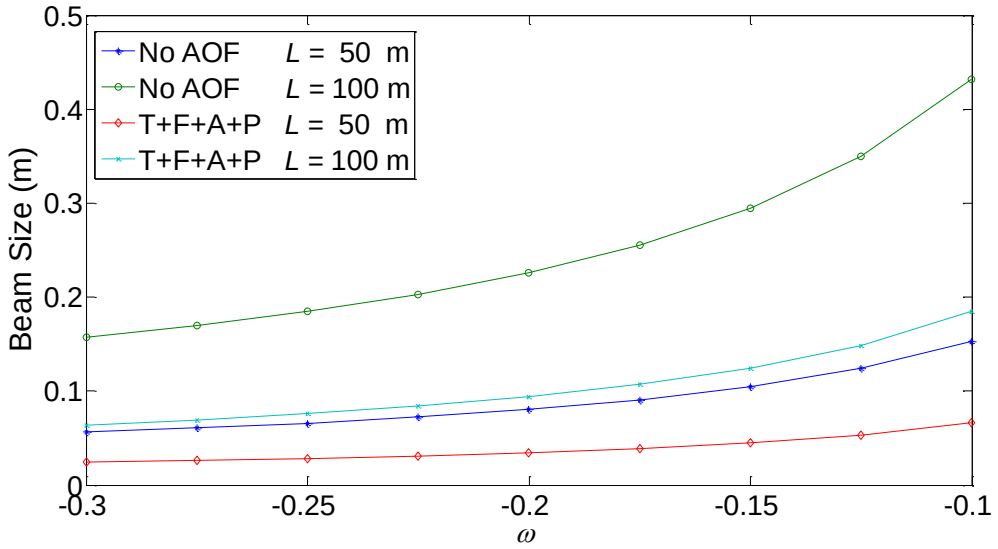

Figure 15: The beam size against ω at various link lengths that use adaptive optics and use with no adaptive optics.

The adaptive optics filter can show its effect more when turbulence is high, so the effect of the filter increases with decreasing ε in Figure 16. The common deduction of Figures 14-16 is that with increasing link length, beam size increases. Also, for larger link length, the sum adaptive optics filter becomes more effective.

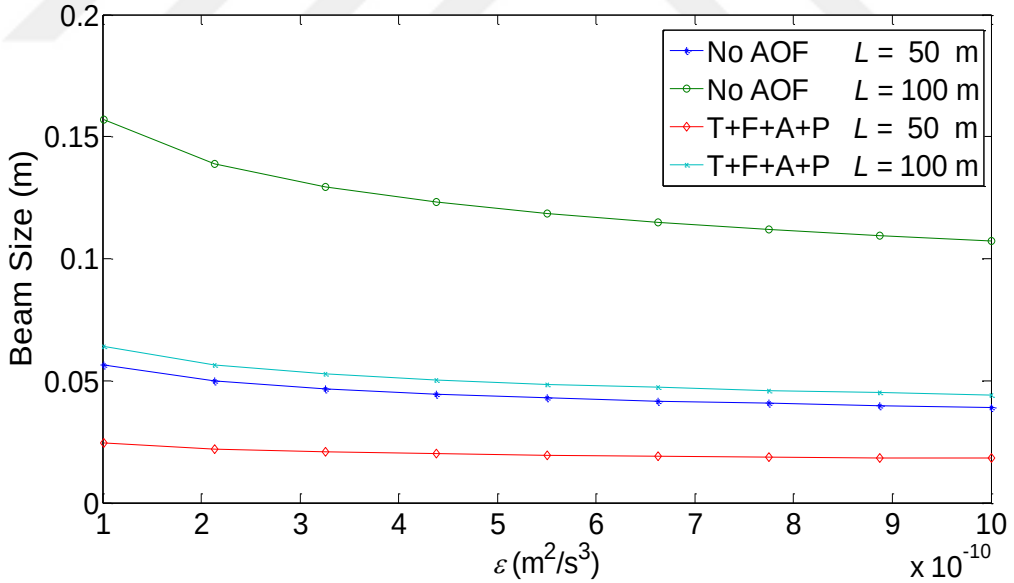

Figure 16: The beam size against ε at various link lengths that use adaptive optics and use with no adaptive optics.

Figure 17 shows that as χ_T increases, beam size increases, and beam size value can be reduced with adaptive optical filter, whatever the value of wavelength

is. For a fixed χ_T, array beam with larger wavelengths expands but both in the case of no AOF and in the case of T+F+A+P the wavelength effect is negligible.

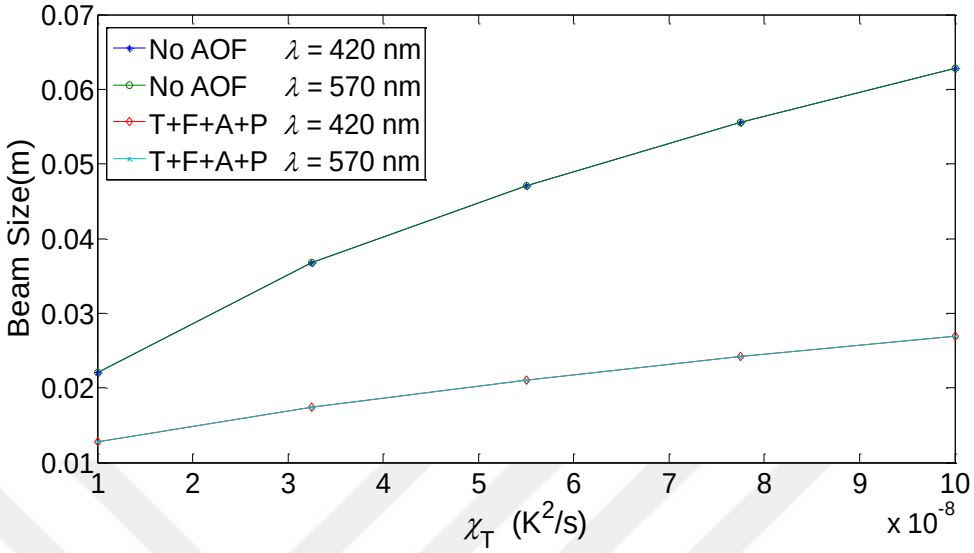

Figure 17: The beam size against χ_T at various wavelengths that use adaptive optics and use with no adaptive optics.

Figure 18 shows that as ω increases, beam size increases and the beam size value can be reduced with adaptive optical filter, whatever the value of wavelength is. In Figure 18, larger beam sizes are observed at the larger wavelength. The change in wavelength had a slight effect on the beam size.

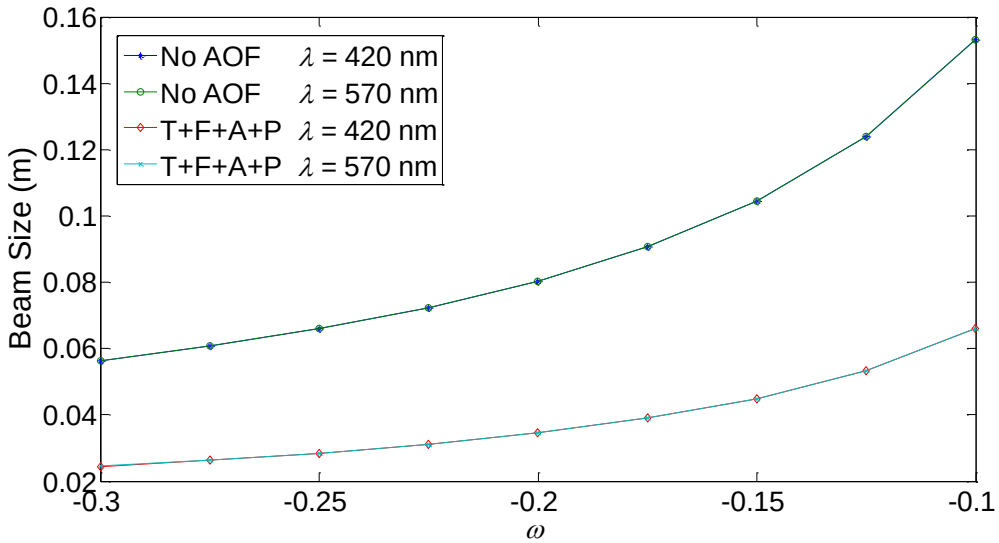

Figure 18: The beam size against ω at various wavelengths that use adaptive optics and use with no adaptive optics.

In Figure 19, beam size increases with decreasing ε value and adaptive optical filter decreases the beam size. Larger wavelength results in larger beam size, but the curves in Figure 17-19 are not indicating this very clearly because for fixed ε, wavelength effect is slight and difference is very small. Also, Figure 17-19 reveal that the reductions of the beam sizes with adaptive optics filter at different wavelengths are almost the same value for any χ_T, ω and ε values.

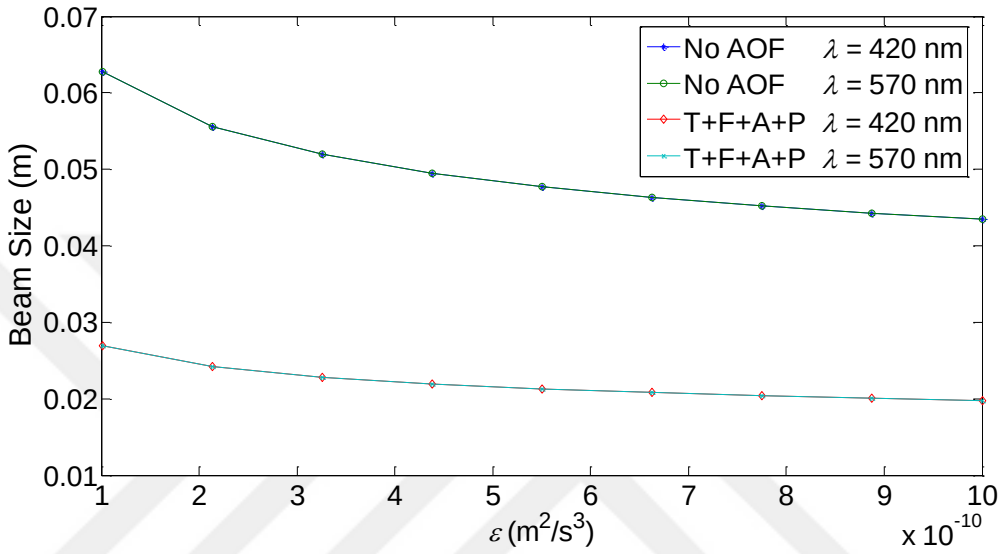

Figure 19: The beam size against ε at various wavelengths that use adaptive optics and use with no adaptive optics.

The beam spread is given in Eq. (3.11). Beam spread is expressed as the difference between the beam size at the receiver for turbulent medium and free space medium.

In Figures 20-23, beam spread due to oceanic turbulence is observed against χ_T, ω and ε at various AO corrections. In Figure 20, with the increase of χ_T temperature field includes large deviations from the mean square temperature so the effects of oceanic turbulence increase and the beam spread increases.

In Figure 20, the graphs indicate the beam spread with no adaptive optics, only tilt corrected (T only), only focus corrected (F only), only astigmatism corrected (A only), only piston corrected (P only) and the sum of tilt, focus, astigmatism and piston corrected (T+F+A+P). If χ_T becomes larger, the beam spread also increases. It is depicted from Figure 20 that for all χ_T, the beam spread is the largest value for with no AO method, and the beam spread is getting smaller respectively, for A only,

F only (the same as A only), T only, P only and for the sum of corrections (T+F+A+P).

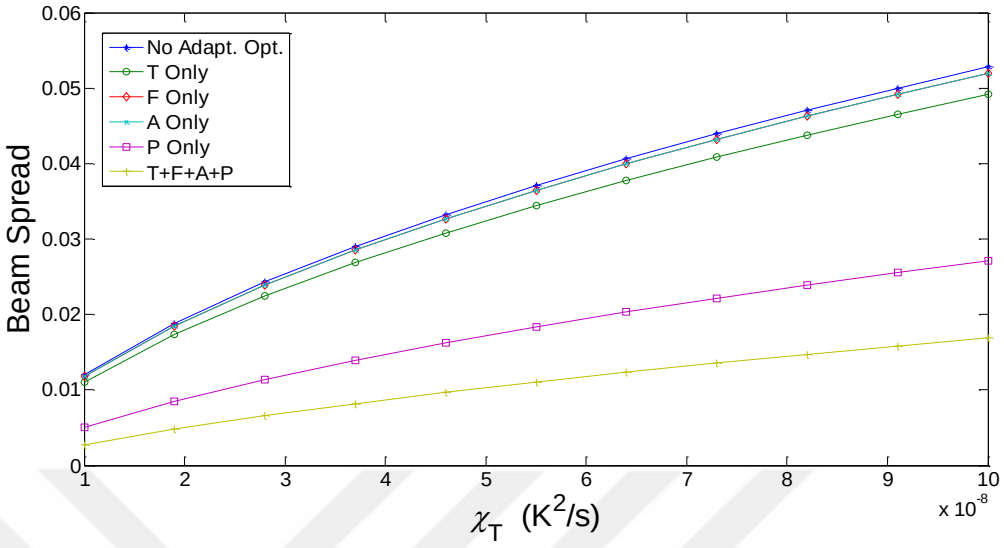

Figure 20: The beam spread against χ_T at various adaptive optics and with no adaptive optics.

It can be seen in Figures 21-23 that increasing χ_T, ω and decreasing ε increase the strength of the ocean turbulence and this causes an increase in the beam spreading. In Figure 21, it can be seen that as ω increases, the beam spread increases for both without AOF and for each filter. Also, the sum of corrections is most effective in reducing the beam spread.

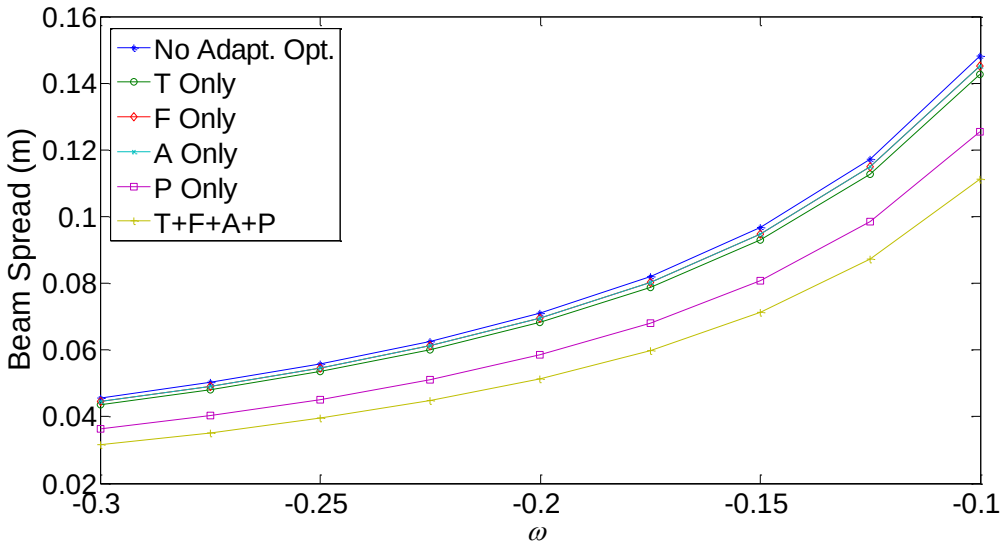

Figure 21: The beam spread against ω at various adaptive optics and with no adaptive optics.

In Figure 22, if ε becomes larger, the beam spread decreases. It is depicted from Figure 22 that for all ε, the beam spread is the largest for without AO correction, and the sequence of the beam spread the beam spread is getting smaller respectively, for A only, F only (the same as A only), T only, P only and for the sum of corrections (T+F+A+P).

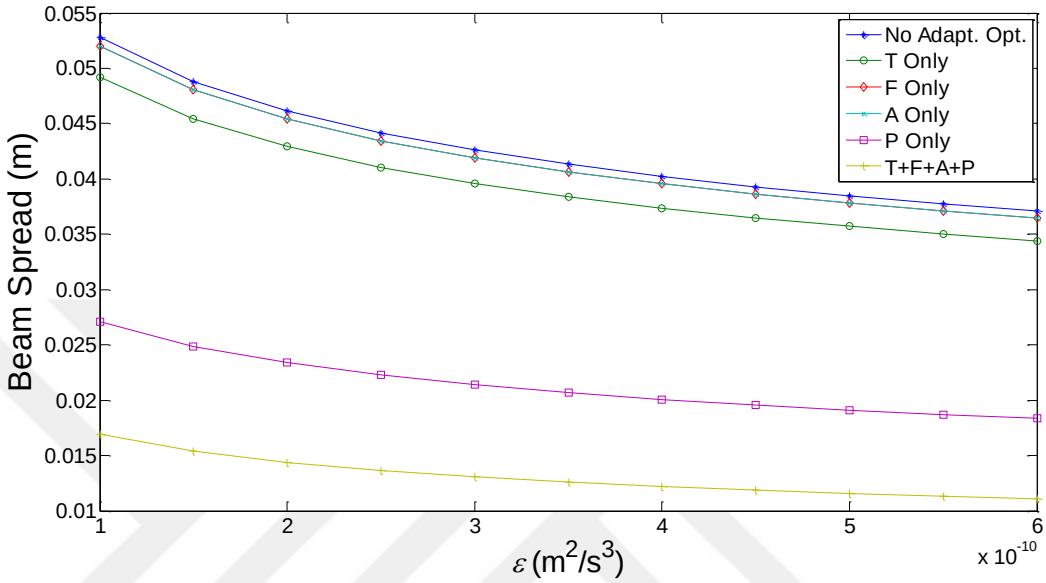

Figure 22: The beam spread against ε at various adaptive optics and with no adaptive optics.

In Figure 23, when the graphs are examined for any χ_T value, it is seen that the beam spread increases as the salinity increases. In addition, the effectiveness of AOF increases with the increase in salinity.

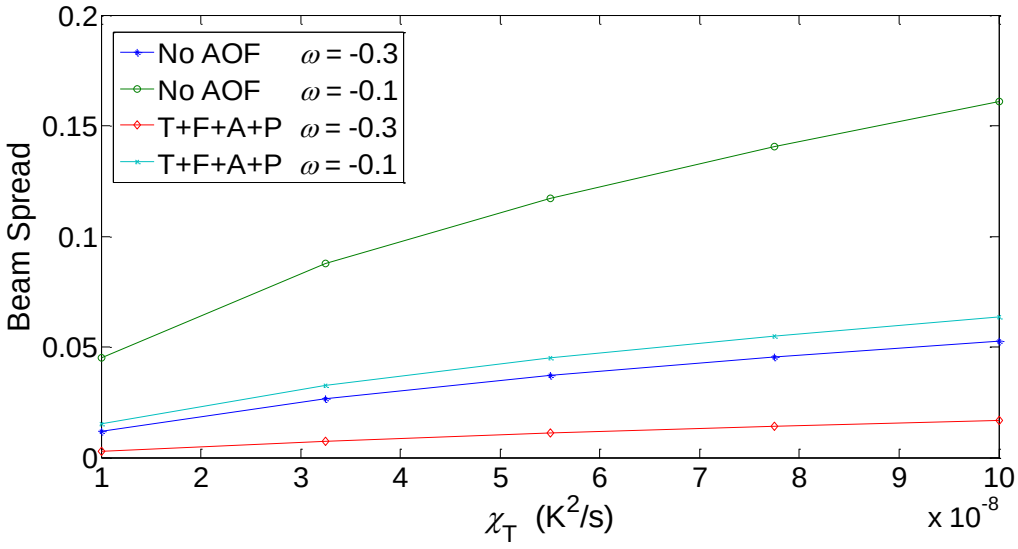

Figure 23: The beam spread against χ_T at various ω that use adaptive optics and use with no adaptive optics.

Figure 24 shows that as the source size increases, beam spread increases. Also, it can be said that the turbulence strength increases when χ_T becomes larger and the effect of adaptive optics correction increases. If we compare the without AO corrected with the sum of the AO corrected curves for $\alpha_s = 0.01$ and for $\alpha_s = 0.15$, we can deduce that adaptive optics correction is more effective at small α_s values.

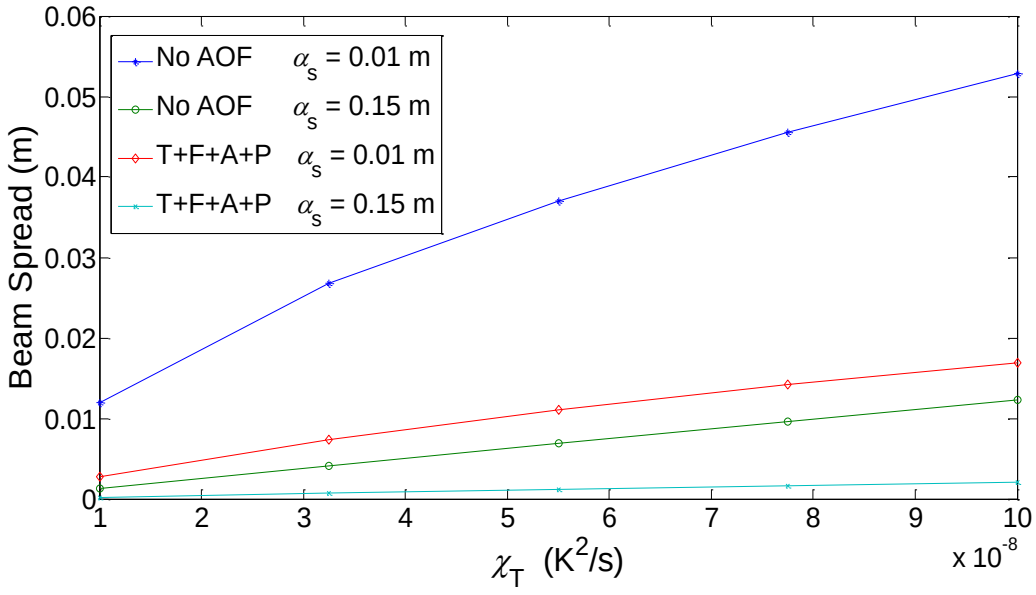

Figure 24: The beam spread against χ_T at various α_s values that use adaptive optics and use with no adaptive optics.

Figure 25 trend is similar to Figure 24 because as χ_T and ω increase, beam spread value increases. As in Figure 24, the difference between no adaptive optics corrected curve and sum of adaptive optics corrected curve for $\alpha_s = 0.01$ is greater than the difference for $\alpha_s = 0.15$ in Figure 25, so it can be deduced that the effectiveness of adaptive optics correction increases as α_s decreases.

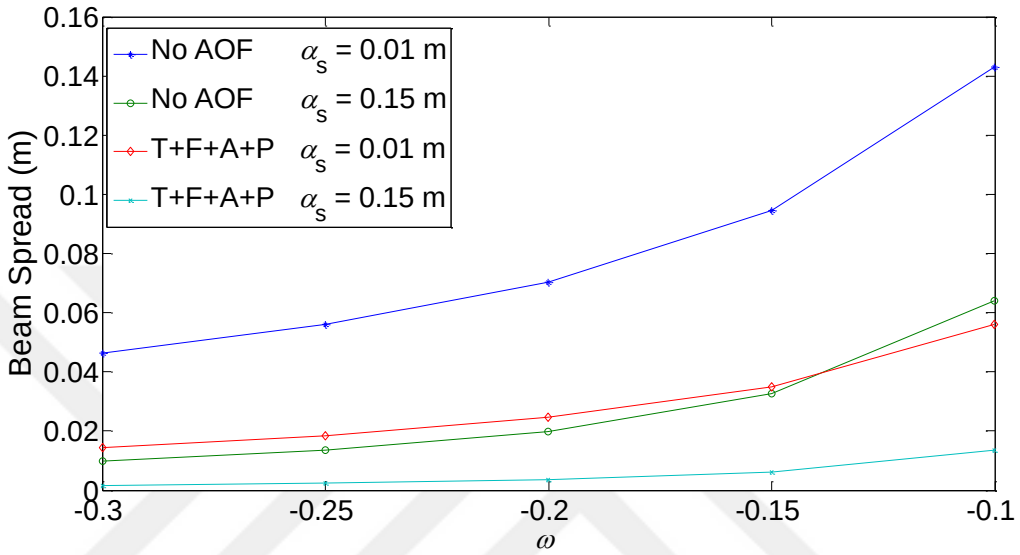

Figure 25: The beam spread against ω at various α_s values that use adaptive optics and use with no adaptive optics.

The effect of turbulence and ε are inversely proportional so increase in ε causes the beam spread to decrease. The curves in Figure 26 show the opposite trend of the curves in Figures 24 and 25. The adaptive optics filter can show its effect more when turbulence strength is high, so the effect of the filter increases with decreasing ε in Figure 26. The common deduction of Figures 24-26 is that with decreasing α_s, beam size decreases, and for small α_s the sum adaptive optics filter becomes more effective.

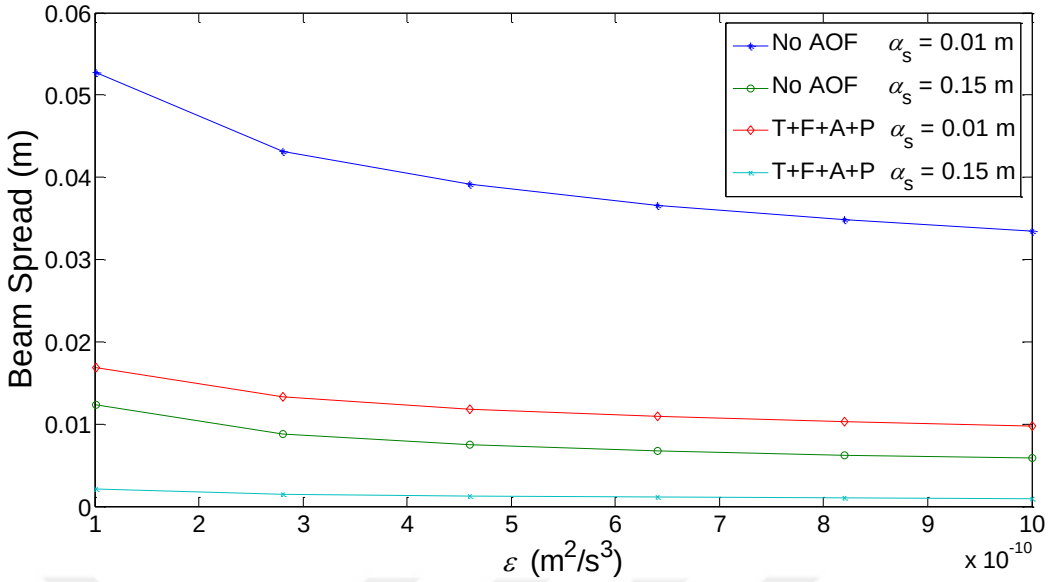

Figure 26: The beam spread against ε at various α_s values that use adaptive optics and use with no adaptive optics.

Figure 27 shows that the beam spread at T+F+A+P against χ_T at various D. Figure 27 shows that for a fixed receiver aperture diameter, larger χ_T causes the larger beam spread. Figure 27 also exhibits that for a constant χ_T, smaller D results in smaller beam spread, namely T+F+A+P for smaller D is most effective at all χ_T values.

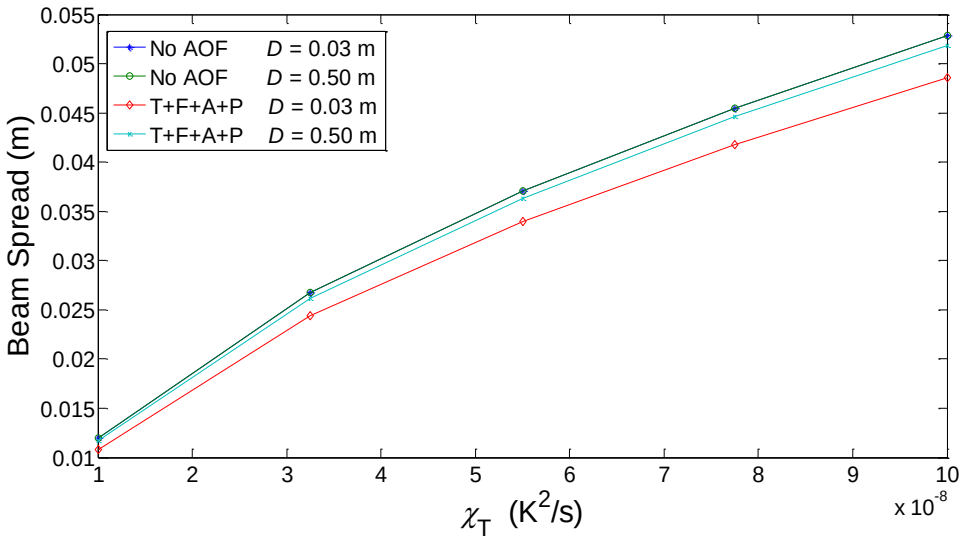

Figure 27: The beam spread against χ_T at various D values that use adaptive optics and use with no adaptive optics.

Figure 28 reflects the beam spread against ω at various D values that use T+F+A+P and use with no adaptive optics. Figure 28 shows that at all D values, larger ω results in larger beam spread. If ω is fixed, smaller receiver aperture diameter yields smaller beam spread and T+F+A+P correction at smaller D value is more effective.

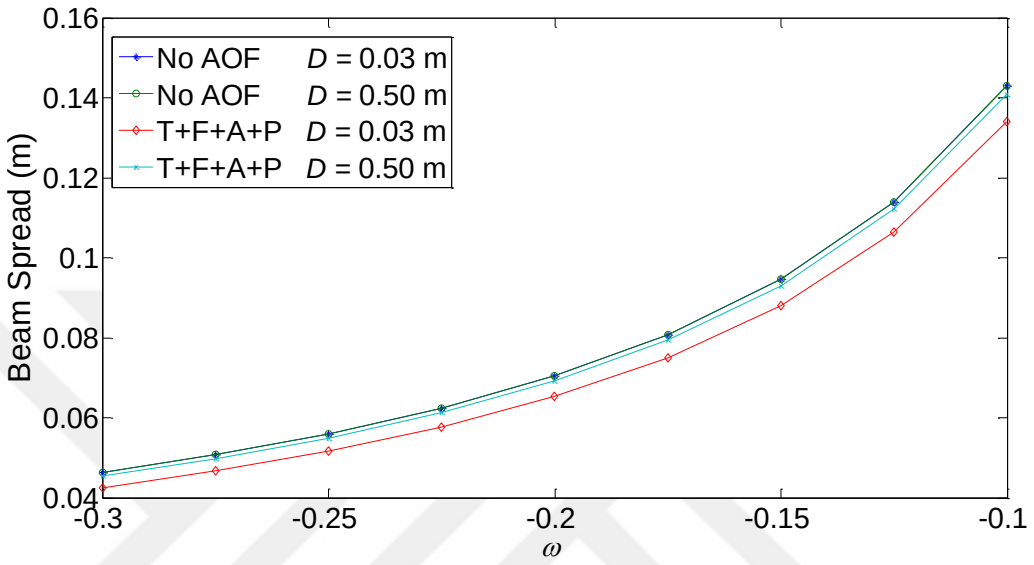

Figure 28: The beam spread against ω at various D values that use adaptive optics and use with no adaptive optics.

Figure 29 shows the beam spread against ε at various D values that use T+F+A+P and use with no adaptive optics.. Figure 29 shows that for a fixed D, smaller ε yields larger beam size and T+F+A+P correction at smaller D is most effective, for every ε.

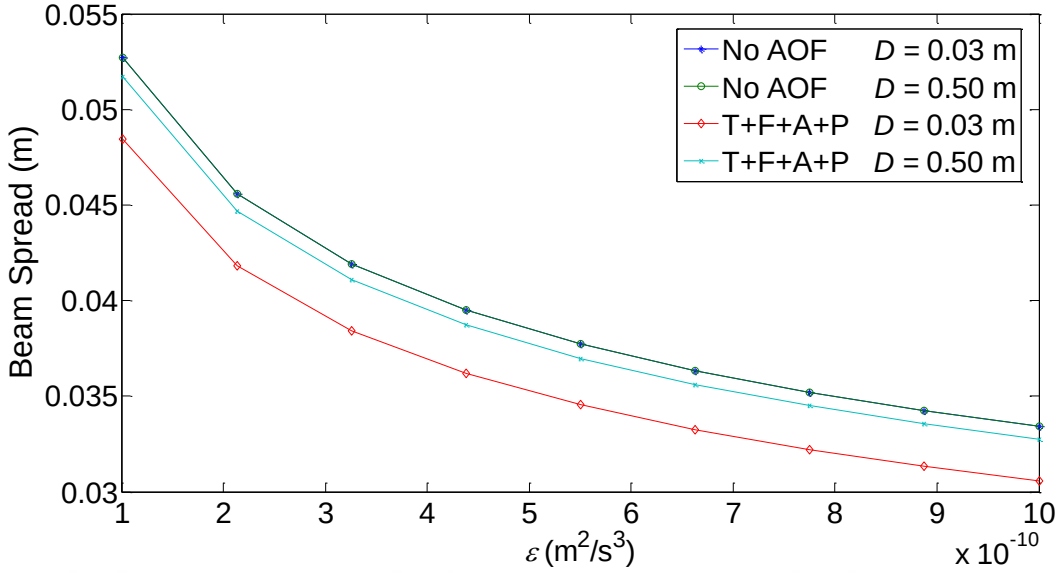

Figure 29: The beam spread against ε at various D values that use adaptive optics and use with no adaptive optics..

Figure 30 shows the beam spread at T+F+A+P adaptive optics correction versus χ_T for different inner scale of the turbulence in oceanic turbulence. Increasing χ_T leads to increase in the beam size value. In Figure 30, it is observed that at any χ_T, larger inner scale yields a decrease in the beam spread so it can be deduced that the effect of T+F+A+P correction increases with the increase of the inner scale value.

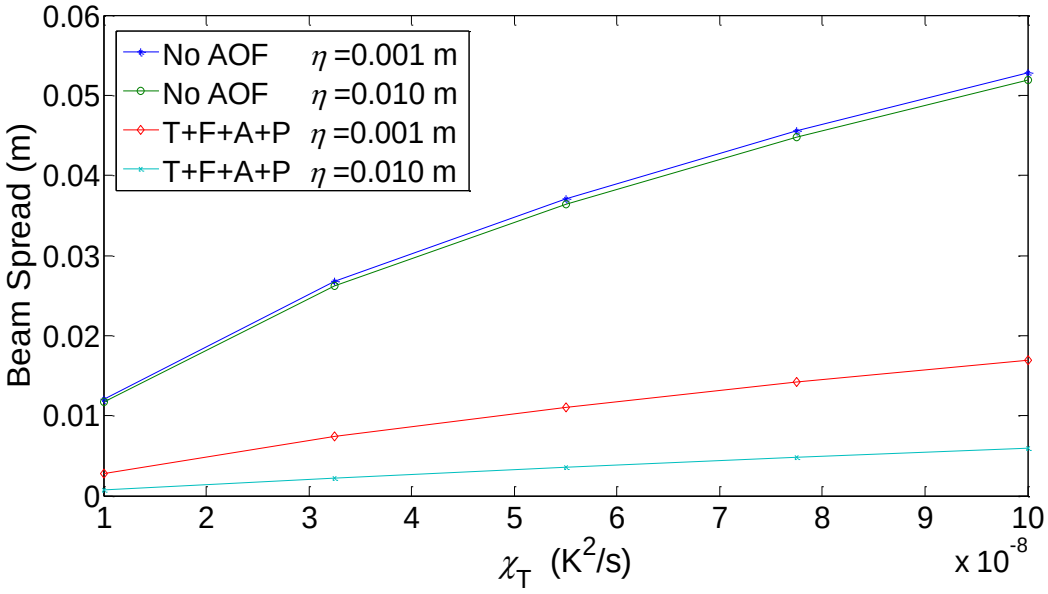

Figure 30: The beam spread against χ_T at various inner scale values that use adaptive optics and use with no adaptive optics.

In Figure 31, T+F+A+P correction is more effective for larger inner scale value. Also, with increasing ω, beam spread increases and the effectiveness of T+F+A+P correction also increases.

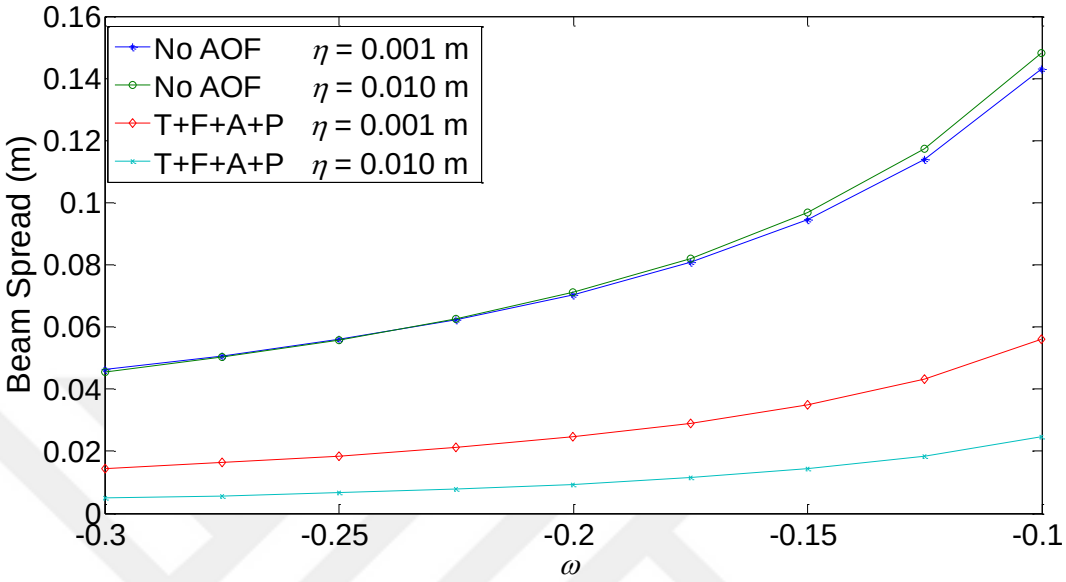

Figure 31: The beam spread against ω at various inner scale values that use adaptive optics and use with no adaptive optics.

Figure 32 shows the beam size at T+F+A+P correction against ε at various inner scale values of oceanic turbulence. The observation is that smaller ε causes the beam spread to increase. Figure 32 also shows that at any ε, larger inner scale value yields a decrease in the beam spread so it can be deduced that the effect of T+F+A+P correction increases with the increase of the inner scale value.

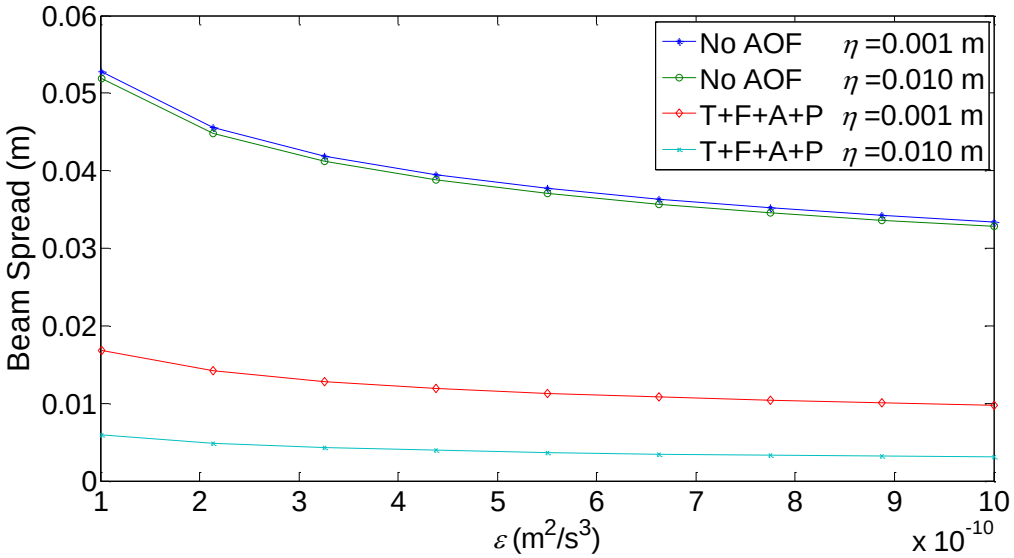

Figure 32: The beam spread against ε at various inner scale values that use adaptive optics and use with no adaptive optics.

Figure 33 exhibits the effectiveness of the AO method against χ_T at various link lengths. For all χ_T values, larger link length results in larger beam spread which means that at a fixed χ_T, the value of the beam spread that use adaptive optics is also larger for larger link lengths. Other observation is that the reduction percentages of the beam spread at several link lengths show the same value at all χ_T. The reduction of the beam spread is larger for the larger link length.

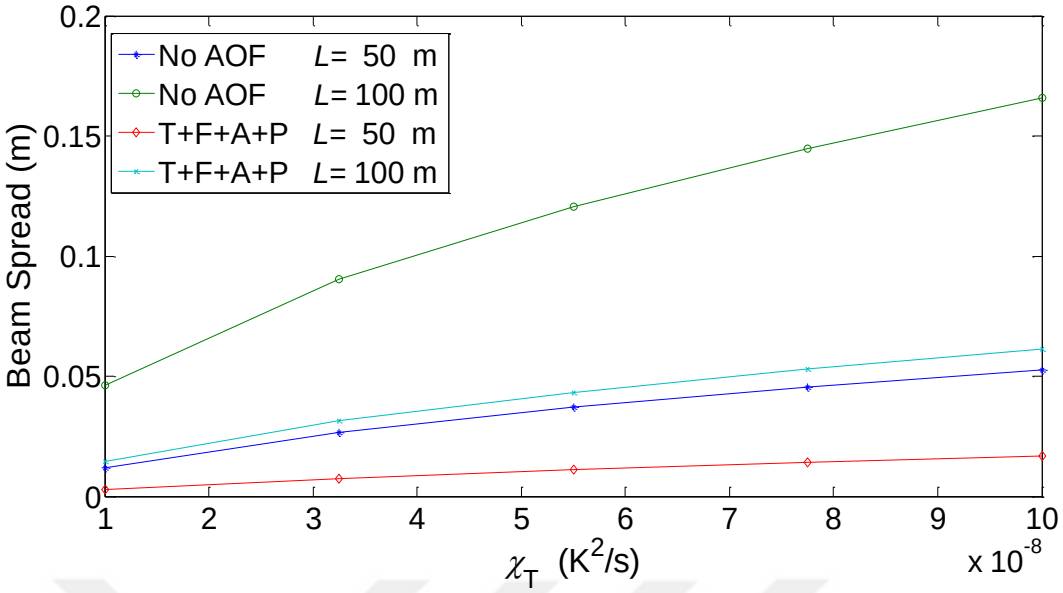

Figure 33: The beam spread against χ_T at various link lengths that use adaptive optics and use with no adaptive optics.

Figure 34 shows the beam spread at T+F+A+P adaptive optics correction versus ω for different link lengths. Increasing ω causes larger beam spread value. In Figure 34, it is observed that at any ω, larger link length yields an increase in the beam spread so it can be deduced that the effect of T+F+A+P correction increases with increasing the link length.

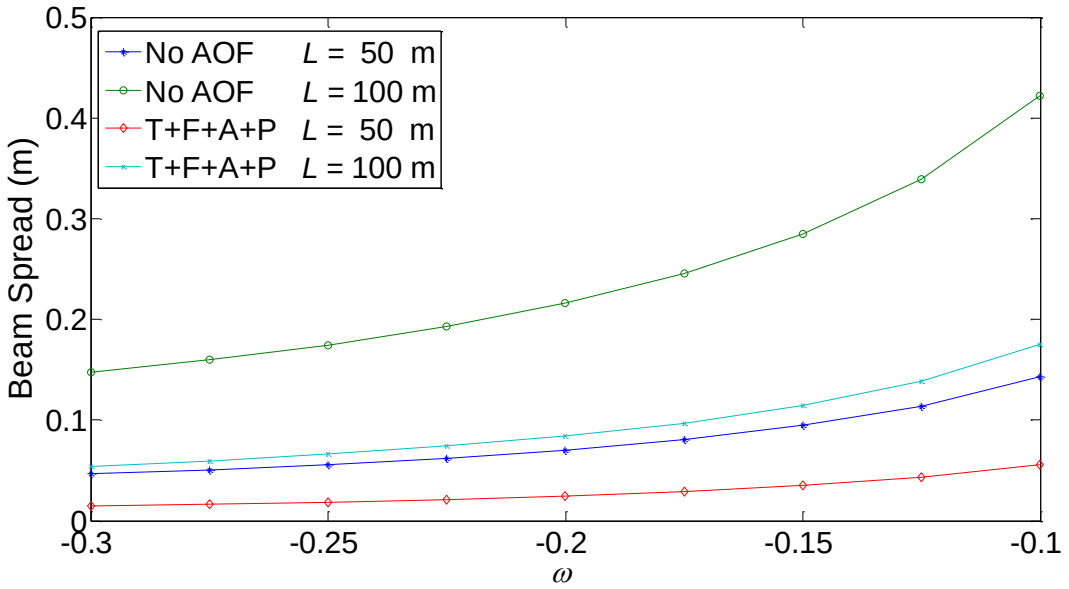

Figure 34: The beam spread against ω at various link lengths that use adaptive optics and use with no adaptive optics.

The adaptive optics filter can show its effect more when turbulence is high, so the effect of the filter increases with decreasing ε in Figure 35. The common deduction of Figures 33-35 is that with increasing link length, beam spread increases. Also, for larger link length, the sum adaptive optics filter becomes more effective.

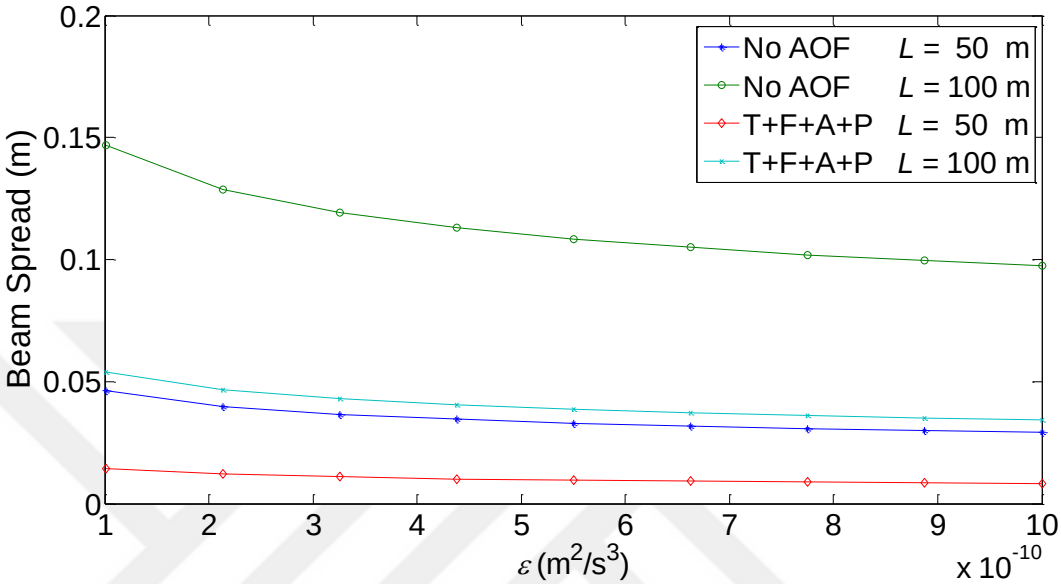

Figure 35: The beam spread against ε at various link lengths that use adaptive optics and use with no adaptive optics.

Figure 36 exhibits that as χ_T increases, beam spread increases, and beam spread value can be reduced with adaptive optical filter, whatever the value of wavelength is. For a fixed χ_T, larger wavelength decreases the beam spread value but both in the case of no AOF and in the case of T+F+A+P the wavelength effect is slight.

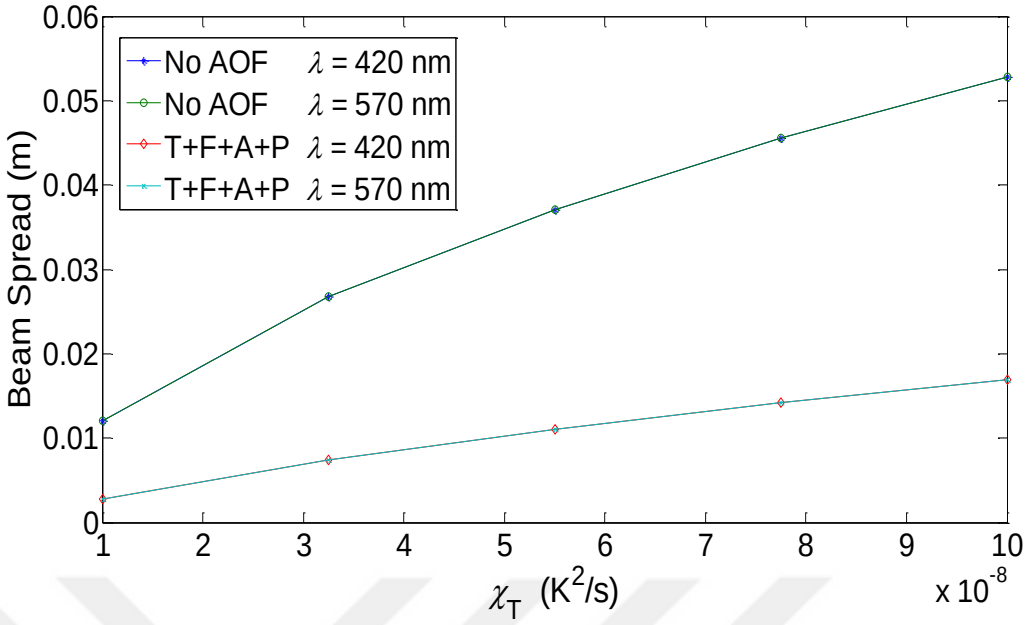

Figure 36: The beam spread against χ_T at various wavelengths that use adaptive optics and use with no adaptive optics.

Figure 37 shows that as ω increases, beam spread increases and the beam spread value can be reduced with adaptive optical filter, whatever the value of wavelength is. In Figure 37, larger beam spread is observed at the smaller wavelength but this difference is very small. Namely, the change in wavelength had a slight effect on the beam spread.

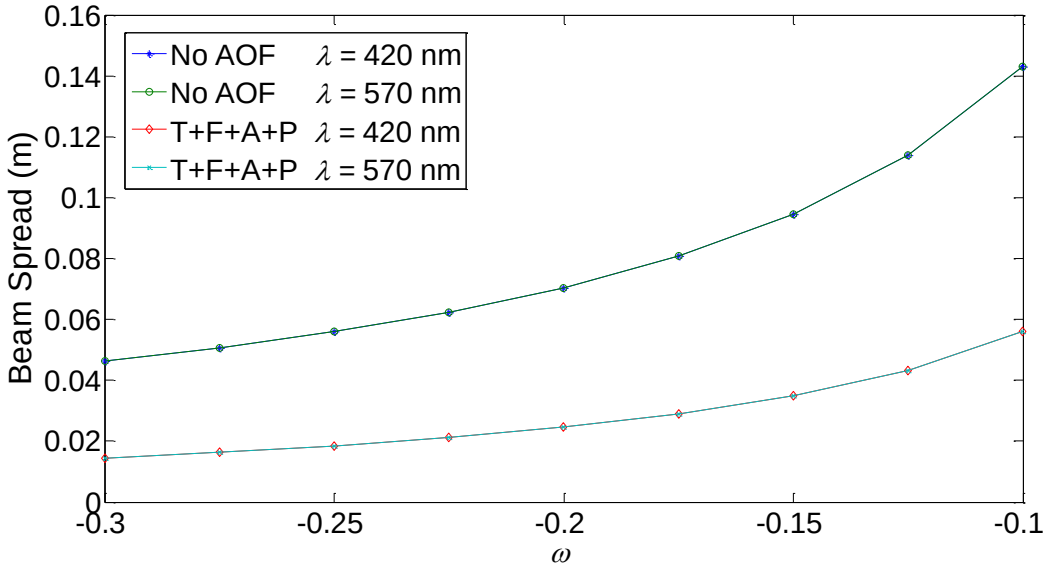

Figure 37: The beam spread against ω at various wavelengths that use adaptive optics and use with no adaptive optics.

In Figure 38, beam spread increases with decreasing ε value and adaptive optical filter decreases the beam spread. Larger wavelength results in smaller beam spread but the curves in Figure 36-38 are not indicating this very clearly because for fixed ε, wavelength effect is slight and difference is very small. Also, Figure 36-38 reveal that the reductions of the beam spread with adaptive optics filter for different wavelengths are almost at the same level at any χ_T, ω and ε values.

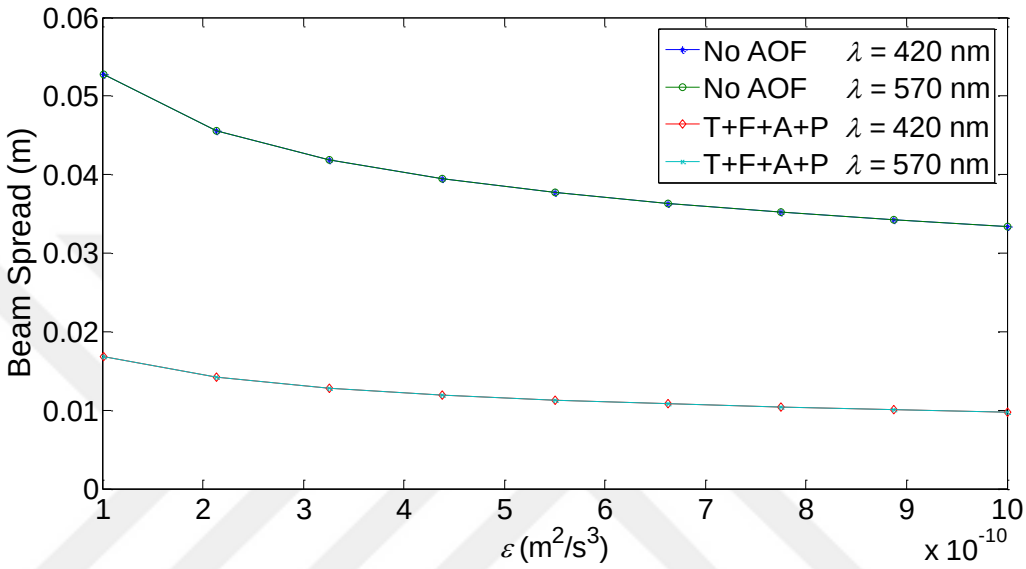

Figure 38: The beam spread against ε at various wavelengths that use adaptive optics and use with no adaptive optics.

CHAPTER 6

CONCLUSION

Underwater turbulence causes the increase in the beam spread which reduces the performance of the UWOC systems. In this thesis, the effectiveness of adaptive optics correction for Gaussian beams in oceanic turbulence is analyzed. The beam size and the beam spread were examined with adaptive optics filters. The reductions in the beam size and the beam spread were achieved with the application of these filters. To investigate the underwater turbulence effect, the power spectrum in the underwater medium is supposed to be isotropic and homogeneous. Using the extended Huygens Fresnel principle, the average intensity is calculated. The beam size and the beam spread were found by the Carter's definition. Piston, tilt, focus, astigmatism and sum of these components of adaptive optics corrections were applied to the beam size and the beam spread in turbulent oceanic medium. The reduction in the beam size and the beam spread was analyzed versus the rate of dissipation of mean squared temperature χ_T, ratio of temperature to salinity contributions to the refractive index spectrum ω, rate of dissipation of kinetic energy per unit mass of fluid ε, inner scale, receiver aperture diameter, link length, source size and the wavelength. This reduction was analysed by comparing the beam spreads that used AO corrections and used with no AO corrections. In this study, it is aimed to provide the most effective conditions during the beam propagation in underwater turbulent environment and to increase the UWOC performance by examining beam spreads using adaptive optics method. Through the employed filter functions of adaptive optics, the reduction of the beam size and the beam spread of the Gaussian beam are evaluated. Adaptive optics correction is utilized in the the beam size and the beam spread with piston only (P only), tilt only (T only), focus only (F only), astigmatism only (A only) and the sum of the T+F+A+P. The influence of the parameters on all the beam spreads was found to be similar. Namely,

as χ_T and ω increase, the strength of oceanic turbulence also increases, but the opposite trend is observed for ε. Therefore, it was seen that only P corrected, only T corrected, only F corrected, only A corrected and the sum of T+F+A+P corrected the beam sizes and the beam spreads, all increase as χ_T and/or ω increase and/or ε decreases. For any underwater turbulence parameters, the reduction in the beam size and the beam spread was analyzed with AO method and with no AO method and this reduction is larger with P only, T only, A only and F only (the same as astigmatism only) corrections, respectively. For this reason, it can be said that the largest reduction in the beam sizes and the beam spreads is achieved if the T+F+A+P correction is utilized. If other link parameters and oceanic turbulence parameters are constant, the reduction in the beam size and the beam spread is observed to be the same whatever ω, χ_T and ε value. Also, for constant oceanic turbulence parameters, smaller D (receiver aperture diameter) provides more effective AO correction. If the effectivenesss of the AO method is compared with the without AO corrected beam size and beam spread, against ω, χ_T and ε, it is observed that at larger link length and at smaller source size and at larger inner scale, AO method becomes more efficient.

The main consequence deduced is that using AO method in underwater optical wireless systems provides reduction in the beam size and beam spread, which will improve the system performance.

REFERENCES

1. THORPE Stephen A. (2007), *"An Introduction to Ocean Turbulence",* Cambridge University Press, Cambridge.
2. HANSON Frank and RADIC Stojan (2008), *"High bandwidth underwater optical communication"*, App. Opt., vol. 47, no. 2, pp. 277-283.
3. ARNON Shlomi and KEDAR Debbie (2009), *"Non-line-of-sight underwater optical wireless communication network"*, J. Opt. Soc. Am. A, vol. 26, pp. 530-539.
4. GABRIEL Chadi, KHALIGHI Mohammad Ali, BOURENNANE Salah, LEON Pierre and RIGAUD Vincent (2013), *"Monte-Carlo-based channel characterization for underwater optical communication systems",* J. Opt. Commun. Netw. vol. 5, pp. 1-12.
5. ARNON Shlomi (2010), "*Underwater Optical Wireless Communication Network*", Opt. Eng., 49, 015001.
6. KAUSHAL Hemani and KADDOUM Georges (2016), *"Underwater Optical Wireless Communication*", IEEE Access, vol. 4, pp. 1518-1547.
7. ZENG Zhaoquan, FU Shu, ZHANG Huihui, DONG Yuhan and CHENG Julian (2017), "*A survey of underwater optical wireless communications*", IEEE Comm. Surv. Tut., vol. 19, pp. 204-238.
8. JOHNSON Laura J., JASMAN Faezah, GREEN Roger J. and LEESON Mark S. (2014), *"Recent advances in underwater optical wireless communications",* Underwater Technol., vol. 32, pp. 167-175.
9. KHALIGHI Mohammad Ali, GABRIEL Chadi, HAMZA Tasnim, BOURENNANE Salah, LEON Pierre and RIGAUD Vincent (2014), *"Underwater wireless optical communication; recent advances and remainingchallenges",* in Proceedings of Transparent Optical Networks, ICTON,pp.1-4.

10. GHASSEMLOOY Zabih, ARNON Shlomi, UYSAL Murat, XU Zhengyuan and CHENG Julian (2015), *"Emerging optical wireless communications-advances and challenges",* IEEE J. Sel. Area Commun., vol. 33, no. 9, pp. 1738-1749.
11. SPAGNOLO Giuseppe Schirripa, COZZELLA Lorenzo and LECCESE Fabio (2020), *"Underwater Optical Wireless Communications: Overview",* Sensors, vol.20, 22
12. ZHANG Yingluo, WANG Yingmin, HUANG Aiping, HU Xin and HAN Fei (2019), *"Influence of eddy diffusivity ratio on Gaussian beam under weak to strong oceanic turbulence",* J. Mod. Opt., vol. 66, pp. 2063-2074.
13. BRUNDAGE Heather (2010), *"Designing a wireless underwater optical communication system",* MSc. thesis, Massachusetts Institute of Technology, Cambridge, MA.
14. SIMPSON Jim Anto (2008), *"A 1Mbps underwater communication system using LEDs and photodiodes with signal processing capability",* MSc. thesis, North California State University, Raleigh, NC.
15. Cossu G., Corsini R., Khalid A. M., Balestrino S., Coppelli A, Caiti A., Ciaramella E., (2013), *"Experimental demonstration of high speed underwater visible light communications",* in Proceedings of IEEE, 2th International Workshop on Optical Wireless Communications (IWOW), Newcastle, United Kingdom, pp. 11-15.
16. ARNON Shlomi., BARRY John R., KARAGIANNIDIS George K., SCHOBER Robert, UYSAL Murat (2012), *"Advanced Optical Wireless Communication",* Cambridge University Press, Cambridge.
17. Doniec M., Vasilescu I., Chitre M., Detweiler C., Hoffmann-Kuhnt M., Rus D., (2009), *"AquaOptical: A lightweight device for high-rate long-range underwater point-to-point communication",* in Proceedings of IEEE, Oceans, pp. 1-6.
18. HANSON Frank and RADIC Stojan (2008), *"High bandwidth underwater optical communication",* App. Opt., vol. 47, no. 2, pp. 277-283.
19. Liu L., Zhou S., Cui J. H., (2008), *"Prospects and problems of wireless communication for underwater sensor networks",* Wirel. Commun. Mob. Com., vol. 8, pp. 977-994.

20. Caiti A., Calabrò V., Munafò A., Dini G., Lo Duca A., (2013), *"Mobile Underwater Sensor Networks for Protection and Security: Field Experience at the UAN11 Experiment",* J. Field Robot., vol. 30, pp. 237-253.
21. Akyildiz F., Pompili D., and Melodia T., (2005), *"Underwater acoustic sensor networks: research challenges",* Ad Hoc Netw. , vol. 33, pp. 255-256
22. STOJANOVIC Milica, PREISIG James (2009), *"Underwater acoustic communication channels: Propagation models and statistical characterization",* IEEE Commun. Mag., vol. 47, pp. 84-89.
23. Chitre, M., Shahabudeen, S., Freitag, L., & Stojanovic, M., (2008), *"Recent advances in underwater acoustic communications & networking",* in Proceedings of IEEE, Oceans, pp. 1-10.
24. MELODIA Tommaso, et. al., (2013), *"Advances in Underwater Acoustic Networking",* pp. 804-852
25. Demirors E., Sklivanitis G., Santagati G. E., Melodia T., Batalama S. N., (2018), *"A high-rate software-defined underwater acoustic modem with real-time adaptation capabilities",* IEEE Access, vol. 6, pp. 18602-18615.
26. Centelles D., Soriano-Asensi A., Martí J. V., Marín R., Sanz P. J., (2019), *"Underwater wireless communications for cooperative robotics with uwsim-net.",* Appl. Sci., vol. 9, 3526.
27. Santos R., Orozco J., Micheletto M., Ochoa S. F., Meseguer R., Millan P., Molina C., (2017), *"Real-time communication support for underwater acoustic sensor networks",* Sensors, vol. 17, 1629.
28. Duntley S. Q., (1963), *"Light in the Sea",* J. Opt. Soc. Am. A, vol. 53, pp. 214-213.
29. Bocus M. J., Doufexi A., Agrafiotis D., (2020), *"Performance of OFDM-based massive MIMO OTFS systems for underwater acoustic communication",* IET Commun., vol. 14, pp. 588-593.
30. DOMINGO Mari Carmen (2011), *"Securing underwater wireless communication networks",* IEEE Wireless Commun., vol. 18, pp. 22-28.
31. Johnson L. J., Jasman F., Green R. J., Leeson M. S., (2014), *"Recent advances in underwater optical wireless communications",* Underwater Technol., vol. 32, pp. 167-175.

32. Saeed N., Çelik A., Al-Naffouri T. Y., Alouini M. S., (2019), *"Underwater optical wireless communications, networking, and localization: A survey",* Ad Hoc Netw., vol. 94, 101935.

33. Jamali M. V., Mirani A., Parsay A., Abdolhassani B., Nabavi P., Chizari A., Khorramshahi P., Abdollahramezani S., Salehi J. A., (2018), *"Statistical Studies of Fading in Underwater Wireless Optical Channels in the Presence of Air Bubble, Temperature, and Salinity Random Variations",* IEEE T. Commun., vol. 66, pp. 4706-4723.

34. Borah D. K., Boucouvalas A. C., Davis C. C., Hranilovic S., Yiannopoulos K., (2012), *"A review of communication-oriented optical wireless systems",* J. Wirel. Commun. Netw., vol. 2012, pp. 1-28.

35. Ghassemlooy Z., Zvanovec S., Khalighi M. A., Popoola W. O., Perez J., (2017), *"Optical wireless communication systems",* Optik, vol. 151, pp. 1-6.

36. Ma H., Liu Y., (2005), *"Correlation based video processing in video sensor networks",* IEEE International Conference on Wireless Networks, Communications and Mobile Computing, vol. 2, pp. 987-992.

37. Spagnolo G. S., Cozzella L., Leccese F., (2019), *"Phase correlation functions: FFT vs. FHT",* ACTA IMEKO, vol. 8, pp. 87-92.

38. Ghassemlooy Z., Uysal M., Khalighi M. A., Ribeiro V., Moll F., Zvanovec S., Belmonte A., (2016), *"An overview of optical wireless communications",* Opt. Wireless Commun., pp. 1-23.

39. Chowdhury M. Z., Shahjalal M., Hasan M., Jang Y. M., (2019), *"The role of optical wireless communication technologies in 5G/6G and IoT solutions: Prospects, directions, and challenges",* Applied Sciences, vol. 9, pp. 4367.

40. ANDREWS Larry C. and PHILIPS Ronald L., HOPEN Cynthia Y., (2001), *"Laser beam scintillation with applications",* SPIE press., vol. 99.

41. Kettle H., Merchant C. J., (2008), *"Modeling ocean primary production: sensitivity to spectral resolution of attenuation and absorption of light",* Prog. Oceanogr., vol. 78, pp. 135-146.

42. Johnson L. J., Green R. J., Leeson M. S., (2013), *"Underwater optical wireless communications: depth dependent variations in attenuation",* Appl. Opt., vol. 52, pp. 7867-7873.

43. MATCIAK Maciej (2012), "*Anomalous diffraction approximation to the light scattering coefficient spectra of marine particles with power law size distribution",* Opt. Express., vol. 20, pp. 27603-27611.

44. SHARIFZADEH Mahsa, AHMADIRAD Mahsa, (2018), *"Performance analysis of underwater wireless optical communication systems over a wide range of optical turbulence",* Opt. Commun., vol. 427, pp. 609-616.

45. OUBEI Hassan M., et. al. (2018), *"Light based underwater wireless communications",* Jpn. J. Appl. Phys., vol. 57, pp. 08PA06/1-18.

46. Stramski D., Boss E., Bogucki D., Voss K. J., (1963), *"The role of seawater constituents in light backscattering in the ocean",* Prog. Oceanogr., vol. 61, no.1, pp. 27-56.

47. Cochenour B., Mullen L., Muth J., (2010), *"Effect of scattering albedo on attenuation and polarization of light underwater",* Opt. Lett., vol 35, pp. 2088-2090.

48. Chen Y., Hu X., Wang D., Chen H., Zhan C., Ren H., (2014), *"Researches on underwater transmission characteristics of blue-green laser",* in Proceedings of IEEE, Oceans, Taipei, Taiwan, pp. 1-5.

49. Kedar D., Arnon S., (2009), *"Subsea ultraviolet solar-blind broadband free-space optics communication",* Opt. Eng., vol. 48, 046001.

50. Darwiesh M., El-Sherif A. F., Ayoub H. S., El-sharkawy Y. H., Hassan M. F., (2018),*"Hyper-Spectral Laser Imaging of Under-Water Targets*", The International Conference on Mathematics and Engineering Physics, vol. 9, pp. 1- 10.

51. Xu J., (2019), *"Underwater wireless optical communication: why, what, and how?",* Chin. Opt. Lett., vol. 17, 100007.

52. Smart J. H., (2005), *"Underwater Optical Communications Systems Part 1: Variability of Water Optical Parameters",* IEEE Milit. Commun. C. (MILCOM 2005), Atlantic City, NJ

53. Conhenour B. M., Mullen L. J., Laux A. E. (2008), *"Characterization of the beam-spread function for underwater wireless communications links",* IEEE J. Oceanic Eng., vol. 33, pp. 513-521.

54. Hanson F., Radic S., (2008), *"High bandwidth underwater optical communication",* Appl. Opt., vol. 47, pp. 277-283.

55. Gabriel C., Khalighi M. A., Bourennane S., Leon P., Rigaud V, (2011),*"Channel Modeling for Underwater Optical Communication",* IEEE GLOBECOM Workshops, Houston, TX.

56. Mobley C., (1994), *"Light and Water",* Academic Press/Elsevier Science, San Diego, CA.

57. Vali Z., Gholami A., Ghasseemlooy Z., Michelson D. G., (2019), *"System Parameters Effect on the Turbulent Underwater Optical Wireless Communications Link"*, Optik, vol. 198, 163153.

58. Wu Y., Zhang Y., Zhu Y., (2016), *"Average intensity and directionality of partially coherent model beams propagating in turbulent ocean",* J. Opt. Soc. Am. A, vol. 33, pp. 1451-1458.

59. Wang Z., Lu L., Zhang P., Qiao C., Zhang J., Fan C., Ji X., (2018), *"Laser Beam Propagation through Oceanic Turbulence",* IntechOpen, http://dx.doi.org/10.5772/intechopen.76894.

60. Nikishov V. V., Nikishov V. I., (2000), *"Spectrum of turbulent fluctuation of the sea water refractive index",* Int. J. Fluid Mech. Res., vol. 27, pp. 82-98.

61. BAYKAL Yahya Kemal (2016), *"Optical Propagation in Unguided Media",* Sig. Com. Tec., pp. 25-45.

62. BAYKAL Yahya Kemal, EYYUBOĞLU Halil T., CAI Yangjian (2019), *"Scintillations of partially coherent multiple Gaussian beams in turbulence",* Appl. Opt., vol. 48, pp. 1943- 1954.

63. ANDREWS Larry C. and PHILIPS Ronald L., (2005), *"Laser Beam Propagation through Random Media, Second Edition",* SPIE Press, Washington.

64. ANDREWS Larry C. (2004), *"Field guide to atmospheric optics",* SPIE.

65. GÖKÇE Muhsin Caner (2012), *"Scintillation analysis and evaluation of Super Lorentz Gaussian laser beams for optical wireless",* MSc. Thesis, Ankara University, Ankara, Turkey.

66. KESKİN Aysan (2020), *"Transmittance, scintillation and BER analysis in underwater optical wireless communication systems",* Ph.D. dissertation, Çankaya University, Ankara, Turkey.

67. KESKİN Aysan, BAYKAL Yahya Kemal (2018), *"On-axis transmittance for partially coherent flat-topped beams in underwater turbulence",* 1st International Eurasian Conf. on Sci. Eng. and Tech., Ankara, Turkey

68. Liu D., Chen L., Wang Y., Wang G., Yin H., (2016), *"Average intensity properties of flat-topped vortex hollow beam propagating through oceanic turbulence",* Optik, vol.127, pp. 6961-6969.

69. Liu D., Wang Y., (2014), *"Evolution behavior of Gaussian-Shell model vortex beams propagating through oceanic turbulence"*, Opt. Express, vol. 22, pp. 17723-17734.

70. Liu D., Wang Y., Zhong H., (2018), *"Average intensity of radial phase locked partially coherent standard Hermite-Gaussian beam in oceanic turbulence",* Opt. Laser Technol., vol. 106, pp. 495-505

71. Liu D., Wang Y., (2018), *"Average intensity of partially coherent Lorentz beams in oceanic turbulence",* Prog. Electromagn. Res. M., vol. 68, pp. 181-191.

72. Liu D., Wang G., Wang Y., (2017), *"Average intensity and coherence properties of a partially coherent Lorentz-Gauss beam propagating through oceanic turbulence",* Opt. Laser Technol., vol. 98, pp. 309-317.

73. Liu D., Wang Y., (2017), *"Average intensity of a Lorentz beam in oceanic turbulence",* Optik, vol. 144, pp. 76-85.

74. Liu D., Wang Y., Wang G. Yin H. M (2018), *"Influences of oceanic turbulence on Lorentz Gaussian beam",* Optik, vol. 154, pp. 738-747.

75. Zhang J., et. al., (2018), *"Effects of the turbulent atmosphere and the oceanic turbulence on the propagation of a rotating elliptical Gaussian beam",* Appl. Phys. B, vol. 124, no. 168.

76. Liu D., Wang G., Yin H., Zhong H., Wang Y., (2019), *"Propagation properties of a partially coherent anomalous hollow vortex beam in underwater oceanic turbulence",* Opt. Commun., vol. 437, pp. 346-354.

77. Liu D., et. al., (2019), *"Average intensity of a partially coherent anomalous hollow beam propagating in underwater oceanic turbulence",* Opt. Appl., vol. 49, pp. 227-239.

78. Liu D., Wang G., Wang Y., Yin H., Zhong H., (2019), *"Radial phased locked multi-Gaussian Schell-model beam array and its properties in oceanic turbulence",* Opt. Laser Technol., vol. 124, 106003.

79. Yousefi M., (2017), *"Analyzing the average intensity distribution and beam width evolution of phase-locked partially coherent radial flat-topped array laser beams in oceanic turbulence",* Laser Phys., vol. 27, pp. 1-14.

80. Wu Y., Zhang Y., Hu Z.D., (2017), *"Effects of oceanic turbulence on the propagation of four-petal Gaussian model beams",* Optik, vol. 129, pp. 93-99.

81. Peng X. F., et. al., (2017), *"Statistical properties of a radially polarized twisted Gaussian Schell-model beam in an underwater turbulent medium",* J. Opt. Soc. Am. A., vol. 34, pp. 133-139.

82. Liu D., Wang Y., (2018), *"Properties of a random electromagnetic multiGaussian Schell-model vortex beam in oceanic turbulence",* Appl. Phys. B, vol. 124, no. 176.

83. Lu L., Wang Z., Zhang J., Zhang P., Qiao C., Fan C., Ji X., (2015), *"Average intensity of M x N gaussian array beams in oceanic turbulence",* Appl. Opt., vol. 54, pp. 7500-7507.

84. Li Y., Han Y., Cui Z., (2019), *"On-axis average intensity of a hollow Gaussian beam in turbulent ocean",* Opt. Eng., vol. 58, 096115.

85. Ma, X., Wang, G., Zhong, H., Wang, Y., Liu, D., (2021), *"The off-axis multi-Gaussian Schell-model hollow vortex beams propagation in free space and turbulent ocean",* Optik, vol. 228, 166180.

86. Huang X., Deng Z., Shi X., Bai Y., Fu X., (2018), *"Average intensity and beam quality of optical coherence lattices in oceanic turbulence withanisotropy",* Opt. Express, vol. 26, pp. 4786-4797.

87. Zhi D., Chen Y. Z., Tao R. M, Ma Y. X., Zhou P., Si L., (2015), *"Average spreading and beam quality evolution of Gaussian array beams propagating through oceanic turbulence",* Laser Phys. Lett., vol. 12, 116001.

88. EYYUBOĞLU Halil T., BAYKAL Yahya Kemal (2004), *"Cosine-Gaussian laser beam intensity in turbulent atmosphere",* Proc. SPIE, vol. 5743, pp. 131-141.

89. EYYUBOĞLU Halil T., BAYKAL Yahya Kemal (2005), *"Average intensity and spreading of cosh-Gaussian laser beams in the turbulent atmosphere",* App. Optics, vol. 44, pp. 976-983.

90. Chu X., Qiao C., Feng X., (2011), *"Average intensity of flattened Gaussian beam in non-Kolmogorov turbulence",* Opt. Laser Technol, vol. 43, pp. 1150-1154.

91. GÖKÇE Muhsin Caner, BAYKAL Yahya Kemal, ATA Yalçın (2020), *"Laser array beam propagation through liver tissue",* J. Visual, vol. 23, pp. 331-338.

92. BAYKAL Yahya Kemal (2022), *"Adaptive optics correction of beam spread in biological tissues",* J. Quant. Spectrosc. Ra., vol. 283, 108145.

93. KESKİN Aysan, BAYKAL Yahya Kemal, ATA Yalçın (2014), *"Optical transmittance in turbulent underwater medium",* Proc. Çankaya Univ., Eng. Tech. Sym., vol. 7, pp. 137- 141.

94. Symth W. D., Moum J. N., (2001), *"3D Turbulence",* College of Oceanic and Atmospheric Sciences Oregon State University, Academic Press, doi:10.1006/rwos.2001.0134.

95. Liang Q., Zhang Y., Yang D., (2020), *"Effects of Turbulence on the Vortex Modes Carried by Quasi-Diffracting Free Finite Energy Beam in Ocean",* J. Mar. Sci. Eng., vol. 8, no. 458.

96. Deng S., Yang D., Zheng Y., Hu L., Zhang, Y., (2014), *"Transmittance of finite-energy frozen beams in oceanic turbulence",* J. Opt. Soc. Am. A., vol. 31, pp. 1552-1556.

97. KESKİN Aysan, BAYKAL Yahya Kemal (2020), *"Effects of underwater turbulence on average transmittance of cos-Gaussian and cosh-Gaussian optical beams",* Wave Random Complex, doi. 10.1080/17455030.2020.1743894

98. ATA Yalçın, BAYKAL Yahya Kemal (2018), *"Anisotropy effect on multi-Gaussian beam propagation in turbulent ocean",* Chin. Opt. Lett., vol. 16, 080102.

99. Keskin A., Çatmakaş O. K., Genç F., Baykal Y., Arpali S. A., Arpali C., (2015), *"Effects of Focused and Collimated Laser Beams on the Performance of Underwater Wireless Optical Communications",* International Workshop on Opt. Wireless Commun., Istanbul, Turkey, pp. 41-45.

100. GÖKÇE Muhsin Caner (2016), *"Beam shaping effects on MIMO free-space optical communication systems",* Ph.D. dissertation, Çankaya University, Ankara, Turkey.

101. ATA Yalçın, BAYKAL Yahya Kemal, (2014), *"Scintillations of optical plane and spherical waves in underwater turbulence",* J. Opt. Soc. Am. A, vol. 31, pp. 1552- 1556.

102. Li Y., Zhang Y., Zhu Y., (2019), *"Oceanic spectrum of unstable stratification turbulence with outer scale and scintillation index of Gaussianbeam wave",* Opt. Express, vol. 27, pp. 7656-7672.

103. Zou Z., et. al., (2019), *"Average capacity of a UWOC system with partiallycoherent Gaussian beams propagating in weak oceanic turbulence",* J. Opt. Soc. Am. A, vol. 36, pp. 1462-1474.

104. Yousefi M., Golmohammady S., Mashal A., Kashani F. D., (2015), *"Analyzing the propagation behavior of scintillation index and bit error rate of partially coherent flat-topped laser beam in oceanic turbulence",* J. Opt. Soc. Am. A, vol. 32, pp. 1982-1992.

105. BAYKAL Yahya Kemal (2015), *"Intensity fluctuations of multimode laser beams in underwater medium",* J. Opt. Soc. Am. A, vol. 32, pp. 593-598.

106. BAYKAL Yahya Kemal (2016), *"Higher order mode laser beam scintillations in oceanic medium",* Wave Random Complex, vol. 26, pp. 21-29.

107. BAYKAL Yahya Kemal (2017), *"Higher order mode laser beam intensity fluctuations in strong oceanic turbulence",* Opt. Commun., vol. 390, pp. 72-75.

108. BAYKAL Yahya Kemal (2016), *"Higher order laser beam scintillation in weakly turbulent marine atmospheric medium",* J. Opt. Soc. Am. A, vol. 33, pp. 758- 763.

109. BAYKAL Yahya Kemal (2016), *"Cross-beam scintillations in underwater medium",* Opt. Eng., vol. 55, 111612.

110. Yousefi M., Kashani F. D., Golmohammady S., Mashal A., (2017), *"Scintillation and bit error rate analysis of a phase-locked partially coherent flat-topped array laser beam in oceanic turbulence",* J. Opt. Soc. Am. A, vol. 34, pp. 2126-2137.

111. GÖKÇE Muhsin Caner, BAYKAL Yahya Kemal, (2016), *"Scintillation analysis of multiple-input single output underwater optical links",* Appl. Opt., vol. 55, pp. 6130-6136.

112. BAYKAL Yahya Kemal (2016), *"Scintillations of LED sources in underwater medium",* Appl. Opt., vol. 55, pp. 8860-8863.

113. Wu Y., Zhang Y., Zhu Y., Hu Z., (2016), *"Spreading and wandering of Gaussian-Schell model laser beams in an anisotropic turbulent ocean",* Laser Phys., vol. 26, no. 09001.

114. Yang Y., Yu L., Wang Q., Zhang Y., (2017), *"Wander of the short-term spreading filter for partially coherent Gaussian beams through the anisotropic turbulent ocean",* Appl. Opt., vol. 56, pp. 7046-7052

115. Niu C., Lu F., Han X., (2019), *"Approximate expression of beam wander of Gaussian array beams through oceanic turbulence",* Optik, vol. 188, pp. 1-7

116. Wu T., Ji X., Li X., Wang H., Deng Y., Ding Z., (2018), *"Characteristics parameters of optical wave and short- term beam spreading in oceanic turbulence",* Acta Phys. Sin., vol. 67, 224206.

117. Charnotskii M., (2015), *"Long and short-term beam spread by turbulence and optimization of the beam geometry",* Oceans IEEE, Genova, ITALY.

118. Tang M., Zhao D., (2015), *"Regions of spreading of Gaussian array beams propagating through oceanic turbulence",* Appl. Opt., vol. 54, pp. 3407-6136.

119. Liu D., Yin H., Wang G., Wang Y., (2017), *"Spreading of a LorentzGauss Vortex Beam Propagating through Oceanic Turbulence",* Curr. Opt. Photon., vol. 3, pp. 97-104.

120. Shirai T., Dogariu A., Wolf E., (2003), *"Mode analysis of spreading of partially coherent beams propagating through atmospheric turbulence",* J. Opt. Soc. Am. A, vol. 20, pp. 1094-1102

121. Zhou, G., (2010), *"Average intensity and spreading of super Lorentz–Gauss modes in turbulent atmosphere",* Appl. Phys. B., vol. 101, pp. 371-379.

122. Zhou G., Chu X., (2010), *"Average intensity and spreading of a Lorentz-Gauss beam in turbulent atmosphere",* Opt. Express., vol. 18, pp. 726-731.

123. Cai Y., He S., (2006), *"Average intensity and spreading of an elliptical Gaussian beam propagating in a turbulent atmosphere",* Opt. Lett., vol. 31, pp. 568-570.

124. Ji X., Zhang E., Lu B., (2006), *"Spreading of partially coherent flattened Gaussian beams propagating through turbulent media",* J. Mod. Opt., vol. 53, pp. 1753-1763.

125. Tang H., Ou B., Luo B., Guo H., Dang A., (2011), *"Average spreading of a radial Gaussian beam array in non-Kolmogorov turbulence",* J. Opt. Soc. Am. A, vol. 28, pp. 1016-1021.

126. Xiao-Ling J., (2010), *"Influence of atmospheric turbulence on the spreading and directionality of radial Gaussian array beams",* Acta Phys. Sin., vol. 59, pp. 692-698.

127. Yi X., Li Z., Liu Z., (2015), *"Underwater optical communication performance for laser beam propagation through weak oceanic turbulence",* Appl. Opt., vol. 54, no. 6, pp. 1273-1278.

128. Gerçekcioğlu H., (2014), "*Bit error rate of focused Gaussian beams in weak oceanic turubulence",* J. Opt. Soc. Am. A, vol. 31, no. 9, pp. 1963- 1968.

129. GÖKÇE Muhsin Caner, BAYKAL Yahya Kemal (2018), *"Aperture averaging and BER for Gaussian beam in underwater oceanic turbulence",* Opt. Commun., vol. 410, pp. 830-835.

130. GÖKÇE Muhsin Caner, BAYKAL Yahya Kemal (2018), *"Aperture averaging in strong oceanic turbulence",* Opt. Commun., vol. 413, pp. 196-199.

131. Peppas K., Boucouvalas A., Ghassemloy Z., (2017), *"Performance of underwater optical wireless communication with multi-pulse pulse-position modulation receivers and spatial diversity",* IET Optoelectron., vol. 11, pp. 180-185.

132. Simpson J. A., Hughes B. L., Muth J. F., (2009), *"A spatial diversity system to measure optical fading in an underwater communications channel",* In Proceedings of IEEE, Oceans, pp. 1-6.

133. Cui Z., Yue P., Yi X., Li J., (2019), *"Scintillation of a partially coherent beam with pointing errors resulting from a slightly skewed underwater platform in oceanic turbulence",* Appl. Opt., vol. 58, pp. 4443-4449.

134. BAYKAL Yahya Kemal (2018), *"Bit error rate of pulse position modulated optical wireless communication links in oceanic turbulence",* J. Opt. Soc. Am. A, vol. 35, pp. 1627-1632.

135. GÖKÇE Muhsin Caner, BAYKAL Yahya Kemal., ATA Yalçın (2018), *"Performance analysis of M-ary pulse position modulation in strong oceanic turbulence",* Opt. Commun., vol. 427, pp. 573-577.

136. GÖKÇE Muhsin Caner, BAYKAL Yahya Kemal., ATA Yalçın (2019), *"Binary phase shift keyingsubcarrier intensity modulation performance in weak oceanic turbulence",* Phys. Commun., vol. 37, 100904.

137. Puent D., (2017), *"Integration of Adaptive Optics into High Energy Laser Modeling and Simulation",* MSc. thesis, Naval Postgraduate School, Monterey, United States.

138. Tyson R. K., (1996), *"Adaptive optics and ground-to-space laser communications",* Appl. Opt., vol. 35, pp. 3640-3646.

139. Tyson R. K., (2002), *"Bit-error rate for free-space adaptive optics laser communications",* J. Opt. Soc. Am. A, vol. 19, pp. 753-758.

140. Liu C., Chen S., Li X., Xian H., (2014), *"Performance evaluation of adaptive optics for atmospheric coherent laser communications",* Opt. Express, vol. 22, pp. 15554-15563.

141. Tyson R. K., Canning D. E., (2003), *"Indirect measurement of a laser communications bit-error-rate reduction with low-order adaptive optics",* Appl. Opt., vol. 42, pp. 4239-4243.

142. Leonhard N., et. al., (2016), *"Real-time adaptive optics testbed to investigate point-ahead angle in pre-compensation of Earth-to-GEO optical communication",* Opt. Express, vol. 24, pp. 13157-13172.

143. Jian H., Ke D., Chao L., Peng Z., Dagang J., Zhoushi Y., (2014), *"Effectiveness of adaptive optics system in satellite-to-ground coherent optical communication",* Opt. Express, vol. 22, pp. 16000-16007.

144. Li J., Zhang Z., Gao J., Sun J., Chen W., (2016), *"Bandwidth of adaptive optics system in atmospheric coherent laser communication",* Opt Commun., vol. 359, pp. 254-260.

145. Liu W, Yao K, Huang D, Lin X, Wang L, Lv Y. (2016), *"Performance evaluation of coherent free space optical communications with a double-*

stage fast-steering-mirror adaptive optics system depending on the Greenwood frequency", Opt. Express, vol. 24, pp. 13288-13302.

146. Wang Y., et. al., (2018), *"Performance analysis of an adaptive optics system for free-space optics communication through atmospheric turbulence",* Sci. Rep., vol. 8, pp. 1-10.

147. Ata Y., Gökçe M. C., Baykal Y., (2020), *"M-ary pulse position modulation performance with adaptive optics corrections in atmospheric turbulence",* J. Mod. Opt., vol. 67, pp. 563-568.

148. Liu W., Yao K., Huang D., Cao J., Wang L., Gu H., (2017), *"Ber analysis of coherent free space optical communication systems with holographic modal wavefront sensor",* Curr. Opt. Photon., vol. 1, pp. 1-6.

149. Toselli I., Gladysz S., (2018), *"Adaptive optics correction of scintillation for oceanic turbulence-affected laser beams",* Proc SPIE, vol. 10787, pp. 45-48.

150. Toselli I., Gladysz S., (2020), *"Improving system performance by using adaptive optics and aperture averaging for laser communications in oceanic turbulence",* Opt. Express, vol. 28, pp. 17347-17361.

151. Baykal Y., Gökçe M. C., Ata Y., (2020), *"Application of adaptive optics on bit error rate of M-ary pulse position modulated oceanic optical wireless communication systems",* Laser Phys., vol. 30, 076202.

152. Baykal Y., (2020), *"*Adaptive *optics correction of scintillation in underwater medium",* J. Mod. Opt., vol. 67, pp. 220-225.

153. Baykal Y., (2020), *"Adaptive optics corrections of scintillations of Hermite-Gaussian modes in an oceanic medium",* Appl Opt., vol. 59, pp. 4826-4832.

154. Gökçe M. C., Baykal Y., Ata Y., (2020), *"Adaptive optics effect on performance of BPSK-SIM oceanic optical wireless communication systems with aperture averaging in weak turbulence",* J. Quant. Spectrosc. Ra., vol. 256, 107335.

155. Tyson R. K., (1982), *"Using the deformable mirror as a spatial filter: application to circular beams",* Appl. Opt., vol. 21, pp. 787–793.

156. Sasiela R. J., (1994), *"Wave-front correction by one or more synthetic beacons",* J. Opt. Soc. Am. A., vol. 11, pp. 379–393.

157. Gradshteyn I. S., Ryzhik M. I., (2007), *"Table of Integrals, Series, and Products",* Academic.

158. Wu Y., Zhang Y., Li Y., Hu Z., (2016), *"Beam wander of Gaussian-Schell model beams propagating through oceanic turbulence"*, Opt. Commun., vol. 371, pp. 59-66.